Roles of Streamwise and Transverse Partial-Vorticity Components in Steady Inviscid Isentropic Supercell-Like Flows

ROBERT DAVIES-JONES

NOAA/National Severe Storms Laboratory, Norman, Oklahoma

(Manuscript received 21 November 2016, in final form 8 May 2017)

ABSTRACT

Investigations of tornadogenesis in supercells attempt to find the origin of the tornado's large vorticity by determining vorticity generation and amplification along trajectories that enter the tornado from a horizontally uniform unstable environment. Insights into tornadogenesis are provided by finding analytical formulas for vorticity variations along streamlines in idealized, steady, inviscid, isentropic inflows of dry air imported from the environment. The streamlines and vortex lines lie in the stationary isentropic surfaces so the vorticity is 2D. The transverse vorticity component (positive leftward of the streamlines) arises from imported transverse vorticity and from baroclinic vorticity accumulated in streamwise temperature gradients. The streamwise component stems from imported streamwise vorticity, from baroclinic vorticity accrued in transverse temperature gradients, and from positive transverse vorticity that is turned streamwise in cyclonically curved flow by a ''river-bend process.'' It is amplified in subsiding air as it approaches the ground. Streamwise stretching propagates a parcel's streamwise vorticity forward in time. In steady flow, vorticity decomposes into baroclinic vorticity and two barotropic parts $\boldsymbol{\omega}_{\mathrm{BTIS}}$ and $\boldsymbol{\omega}_{\mathrm{BTIC}}$ arising from imported storm-relative streamwise vorticity (directional shear) and storm-relative crosswise vorticity (speed shear), respectively. The Beltrami vorticity $\boldsymbol{\omega}_{\mathrm{BTIS}}$ is purely streamwise. It explains why abundant environmental storm-relative streamwise vorticity close to ground favors tornadic supercells. It flows directly into the updraft base unmodified apart from streamwise stretching, establishing mesocyclonic rotation and strong vortex suction at low altitudes. Increase (decrease) in storm-relative environmental wind speed with height near the ground accelerates (delays) tornadogenesis as positive (negative) $\boldsymbol{\omega}_{\mathrm{BTIC}}$ is turned into streamwise (anti-streamwise) vorticity within cyclonically curved flow around the mesocyclone.

1. Introduction

Vorticity dynamics is fundamental to understanding tornadogenesis (see reviews by Davies-Jones et al. 2001, hereafter DJ+01; Davies-Jones 2015a). Dutton (1986) showed theoretically that the vorticity of a parcel in inviscid, isentropic flow decomposes into barotropic and baroclinic parts. By using propagators, Epifanio and Durran (2002) and Davies-Jones (2006, 2015b) extended this work to include vorticity arising from frictional torques, planetary vorticity, and modifications owing to diabatic heating and thermal diffusion. Epifanio and Durran used their theory to explain orographic vortices. Davies-Jones and Brooks (1993, hereafter DJB93) applied Dutton's decomposition to mesocyclogenesis. Circulation around a closed material circuit is closely related to vorticity following parcels. Rotunno and Klemp (1985, hereafter RK85), DJB93, and others in simulated supercells and Markowski et al. (2012) and others in observed supercells have computed the circulation around material circuits. At a time t_1 the circuits are horizontal, close to the ground, and tightly enclose maxima of vertical vorticity. They are then traced backward via trajectories to an earlier time t_0. Since barotropic circulation is conserved (Kelvin's theorem), gains in circulation between t_0 and t_1 are attributed to nonbarotropic (mainly baroclinic) circulation. In a related approach, Adlerman et al. (1999), Dahl et al. (2014), and Markowski and Richardson (2014, hereafter MR14) computed the vorticity budgets of individual parcels that enter the near-ground vorticity maximum. These and most other studies conclude that rotation near the ground in supercells originates in outflow air with baroclinic vorticity and even frictional vorticity (Schenkman et al. 2014). The environmental barotropic vorticity appears to play only a minor role at best. However, as stated by MR14, there are two pieces of

Corresponding author: Dr. Robert Davies-Jones, bobdj1066@yahoo.com

DOI: 10.1175/JAS-D-16-0332.1

evidence that seem inconsistent with the above conclusions. First, tornadogenesis is more likely to occur in supercells having weak cold pools rather than strong cold pools (Markowski et al. 2002). Thus, too much baroclinity seems to be bad for tornadogenesis. This may be due simply to air in the outflow being too heavy for the updraft to lift. Second, proximity soundings (e.g., Markowski et al. 2003a) indicate that the presence of abundant near-ground environmental vorticity that is mainly streamwise in the storm-relative frame favors tornadic supercells. Confusingly, tornadic vorticity derives mainly from storm-induced baroclinic vorticity, but in spite of this, tornadogenesis is affected by environmental vorticity.

In theoretical studies exact solutions of the governing equations are useful. There are Beltrami-flow exact solutions that model updraft rotation and linear propagation of a midaltitude updraft in an environment with a circular hodograph (Lilly 1982; Davies-Jones 2002, 2004; Davies-Jones and Richardson 2002). In a Beltrami flow the vorticity and velocity vectors are parallel in a reference frame moving with the storm. Davies-Jones (2008, hereafter DJ08) used this mesocyclone model as the initial condition in an axisymmetric simulation that produced tornadoes after the initial balanced flow was upset by falling precipitation, and Kis et al. (2008) extended this work to three dimensions. The experiment in DJ08 demonstrated that tornadoes can originate from barotropic vorticity because the model's axisymmetry prevented baroclinic vorticity from being tipped into the vertical. Although inviscid Beltrami flows are inherently steady and exclude buoyancy forces, their characteristics are still conspicuous in actual and simulated supercells in environments with highly curved hodographs (Davies-Jones 1984, 2002, 2004; Lilly 1986). Even in environments where the vorticity is significantly positive crosswise (left normal to the wind), the vorticity entering the tornadic region of the storm can still end up predominantly streamwise (MR14) owing to the "river-bend effect," which turns positive crosswise vorticity into the streamwise direction in left-turning flow (Shapiro 1972; Scorer 1997; DJ+01).

An outstanding tornadogenesis problem is how significant vertical vorticity appears at the ground. Concentrated vortices contact the ground even in simulations completely devoid of background vertical vorticity. The development of near-ground vertical vorticity in these simulations is possible only in air that has previously descended (Davies-Jones 1982, 2000; DJB93; Adlerman et al. 1999; DJ+01; Davies-Jones and Markowski 2013). The conceptual model of DJB93 explains roughly how air with streamwise barotropic vorticity that flows through a downdraft might acquire vertical vorticity next to the ground. In a downdraft with a transverse temperature gradient, generation of horizontal vorticity causes vortex lines to be inclined upward relative to the streamlines. Consequently, there is cyclonic vorticity at the nadirs of the streamlines as they exit the downdraft. Davies-Jones (2000, hereafter DJ00) developed an analytical model that quantified the DJB concepts. This model is discussed further in section 4.

The DJ00 treatment involved a number of simplifications such as the primary–secondary flow decomposition and low-speed, irrotational primary flow with essentially straight streamlines. Without making these assumptions, the theory presented below discovers in natural coordinates analytical formulas for how barotropic and baroclinic vorticity varies along streamlines in steady, inviscid, isentropic inflows of dry air with zero potential vorticity (PV) from the environment and yields some new results. The paper differs from previous work by defining streamwise vorticity as the vorticity parallel to the 3D wind and transverse vorticity as the component in the local isentropic surface that is directed 90° to the left of the streamline. Transverse is used instead of crosswise to remind the reader that the direction is generally nonhorizontal. The transverse and crosswise directions are the same in an undisturbed horizontally uniform environment. Since the PV is zero, there is no component normal to the isentropic surface. In steady flow, vertical vorticity can exist at the nadir point of a streamline only if there is a transverse component of vorticity.

2. General relationships for steady isentropic flow

In a reference frame moving with uniform velocity, consider steady, inviscid, isentropic flow of dry air. Let the scale of the flow be small enough for Coriolis effects to be negligible (Rossby number $\gg 1$) and let the specific dry entropy $S(Z)$ be a function only of the conserved variable Z that is defined in the next section. Then the equations governing motion, mass continuity, and entropy are

$$\boldsymbol{\omega} \times \mathbf{v} + \nabla B = T \frac{dS}{dZ} \nabla Z, \tag{1}$$

$$\nabla \cdot (\mathbf{v}\alpha_0/\alpha) = 0, \quad \mathbf{v} \cdot \nabla \alpha_0 = 0, \quad \text{and} \tag{2}$$

$$\mathbf{v} \cdot \nabla Z = 0, \tag{3}$$

respectively, where $(dS/dZ)\,\nabla Z \equiv \nabla S$, $\mathbf{v}$ is the storm-relative wind, $\boldsymbol{\omega}$ is the vorticity, $\alpha \equiv 1/\rho$ is the specific volume, ρ is density, T is temperature, g is gravitational acceleration, z is height, c_p is the specific heat of dry air at constant pressure, $B \equiv \mathbf{v}\cdot\mathbf{v}/2 + c_pT + gz$ is the

Bernoulli function, $\boldsymbol{\omega} \times \mathbf{v}$ is the Lamb vector $\mathbf{L}$, and $\alpha_0 > 0$ is a conserved specific volume (specified in section 3). From now on the wind is tacitly the relative one since there is only one reference frame in which the flow can be steady. By definition,

$$\boldsymbol{\omega} = \nabla \times \mathbf{v}. \tag{4}$$

Entropy is related to T and α by

$$S = c_v \ln T + R \ln \alpha + \text{const.}, \tag{5}$$

where R is the gas constant for dry air and $c_v = c_p - R$ is the specific heat of dry air at constant volume (Dutton 1986, p. 47). Equation (1) is Crocco's theorem (Batchelor 1967, p. 160) and (1)–(5) are a closed set in the variables $\mathbf{v}$, $\boldsymbol{\omega}$, T, Z, α, and α_0. By virtue of (2) and (3), there exists a streamfunction ψ such that

$$\mathbf{v} = a\nabla\psi \times \nabla Z, \tag{6}$$

where $a \equiv \alpha/\alpha_0$ is a dilatation ratio. The steady-state vorticity equation, the curl of (1), is

$$\nabla \times (\boldsymbol{\omega} \times \mathbf{v}) = \nabla T \times \nabla S. \tag{7}$$

With use of vector identities and (2), the vorticity equation may be reformulated as

$$(\mathbf{v} \cdot \nabla)(a\boldsymbol{\omega}) - (a\boldsymbol{\omega} \cdot \nabla)\mathbf{v} = a\nabla T \times \nabla S. \tag{8}$$

In a barotropic atmosphere ($\nabla T \times \nabla S \equiv 0$), a solution of (8), (2), and (4) is the Beltrami one, $\alpha\boldsymbol{\omega} = \lambda\mathbf{v}$ where $\mathbf{v} \cdot \nabla\lambda = 0$.

From $\mathbf{v} \cdot (1)/a$, (3), and (6),

$$0 = \rho\mathbf{v} \cdot \nabla B = (\nabla\psi \times \nabla Z) \cdot \nabla B, \tag{9}$$

which implies that B is at most a function of ψ and Z [symbolically $B = B(\psi, Z)$]. Thus,

$$\nabla B = \frac{\partial B}{\partial \psi}\nabla\psi + \frac{\partial B}{\partial Z}\nabla Z. \tag{10}$$

Next we introduce Ertel's potential vorticity Q, which is defined here by

$$Q \equiv a\boldsymbol{\omega} \cdot \nabla Z. \tag{11}$$

In appendix A we prove that

$$\mathbf{v} \cdot \nabla Q = 0 \tag{12}$$

(constancy of PV along streamlines), which implies that

$$(\nabla\psi \times \nabla Z) \cdot \nabla Q = 0 \tag{13}$$

and, hence, that $Q = Q(\psi, Z)$. We now need the identity for the vector triple product

$$\mathbf{V}_1 \times (\mathbf{V}_2 \times \mathbf{V}_3) \equiv (\mathbf{V}_1 \cdot \mathbf{V}_3)\mathbf{V}_2 - (\mathbf{V}_1 \cdot \mathbf{V}_2)\mathbf{V}_3. \tag{14}$$

By (6), (14), and (11), the Lamb vector

$$\mathbf{L} \equiv \boldsymbol{\omega} \times \mathbf{v} = a\boldsymbol{\omega} \times (\nabla\psi \times \nabla Z) = Q\nabla\psi - Q^*\nabla Z, \tag{15}$$

where $Q^* \equiv a\boldsymbol{\omega} \cdot \nabla\psi$. With (10) and (15), the equation of motion [(1)] becomes

$$\left(Q + \frac{\partial B}{\partial \psi}\right)\nabla\psi = \left(Q^* - \frac{\partial B}{\partial Z} + T\frac{dS}{dZ}\right)\nabla Z. \tag{16}$$

Since $\nabla\psi$ and ∇Z are not parallel when $\mathbf{v} \neq \mathbf{0}$ [see (6)], we must have

$$T\frac{dS}{dZ} - \frac{\partial B}{\partial Z} = -Q^* \tag{17}$$

and

$$Q = -\partial B/\partial\psi. \tag{18}$$

Kanehisa (1996) and DJ00 previously derived (18). From $a\boldsymbol{\omega} \cdot$ (1) and (11),

$$a\boldsymbol{\omega} \cdot \nabla B = T\frac{dS}{dZ}Q. \tag{19}$$

From (3), the streamlines lie in the isentropic surfaces. Dutton (1986, 387–390) showed that the vorticity $\boldsymbol{\omega}$ in isentropic flow decomposes into a barotropic part $\boldsymbol{\omega}_{\mathrm{BT}}$ and a baroclinic part $\boldsymbol{\omega}_{\mathrm{BC}}$. With this decomposition, we can partition (7) into $\nabla \times (\boldsymbol{\omega}_{\mathrm{BT}} \times \mathbf{v}) = 0$ and $\nabla \times (\boldsymbol{\omega}_{\mathrm{BC}} \times \mathbf{v}) = \nabla T \times \nabla S$. The baroclinic vortex lines lie in the isentropic surfaces and so the baroclinic vorticity does not contribute to PV. Since $a\boldsymbol{\omega}_{\mathrm{BT}}$ satisfies the homogeneous version of (8), the barotropic part of $a\boldsymbol{\omega}$ is frozen into the fluid (Borisenko and Tarapov 1979, p. 240). We assume from now on that the steady inviscid isentropic flow has zero PV ($Q = 0$). Consequently, $B = B(Z)$ from (10) and (18). Thus, the Bernoulli surfaces (of constant B) coincide with the constant-Z and isentropic surfaces. Hence from (19) with $Q = 0$ the barotropic vortex lines also lie in the isentropic surfaces. Moreover, from (15), (10), and (18), $\mathbf{L}$ and ∇B are both normal to these surfaces, and from (1), $B = B(Z)$, and (17),

$$\mathbf{L} \equiv \boldsymbol{\omega} \times \mathbf{v} = \left(T\frac{dS}{dZ} - \frac{dB}{dZ}\right)\nabla Z = -Q^*\nabla Z. \tag{20}$$

We call a function that is like a streamfunction, but for vorticity instead of velocity, a vortex-line function. Since the baroclinic vortex lines lie in the Z surfaces

and for a zero-PV flow the barotropic vortex lines also lie in these surfaces, there exist vortex-line functions Λ, M, and χ for baroclinic, barotropic, and total vorticities such that

$$\boldsymbol{\omega}_{\mathrm{BC}} = \nabla\Lambda \times \nabla S, \quad \boldsymbol{\omega}_{\mathrm{BT}} = \nabla M \times \nabla Z, \quad \boldsymbol{\omega} = \nabla\chi \times \nabla Z, \tag{21}$$

where $\chi \equiv M + \Lambda\, dS/dZ$. Note that $\nabla \cdot \boldsymbol{\omega}_{\mathrm{BT}} = \nabla \cdot \boldsymbol{\omega}_{\mathrm{BC}} = 0$ as required of partial vorticities. In the constant-Z surfaces the total, barotropic, and baroclinic vortex lines are everywhere parallel to the isopleths of χ, M, and Λ, respectively. The advection of χ equals Q^* since

$$\begin{aligned} -\mathbf{v} \cdot \nabla\chi &= -a(\nabla\psi \times \nabla Z) \cdot \nabla\chi \\ &= a(\nabla\chi \times \nabla Z) \cdot \nabla\psi = a\boldsymbol{\omega} \cdot \nabla\psi = Q^* \end{aligned} \tag{22}$$

by (6), (21), and a vector identity. In appendix A we find the equation [(A2)] that Q^* satisfies and prove that its barotropic part $Q^*_{\mathrm{BT}} \equiv a\boldsymbol{\omega}_{\mathrm{BT}} \cdot \nabla\psi$, is constant along each streamline.

3. The environment

As in many supercell simulations without the Coriolis force, we may assume a horizontally uniform environment from which parcels enter the storm. In this far field, the streamlines and vortex lines are effectively horizontal and lie in surfaces of constant Z where Z is the height of parcels far upstream. In a homentropic (constant S) atmosphere, the material constant-Z surfaces exist by themselves. In a stratified atmosphere with monotonic $S(Z)$, the isentropic surfaces coincide with the constant-Z surfaces. In either case, the PV is zero in the environment and hence zero everywhere by PV conservation. We use subscript 0 to denote environmental quantities (apart from use of Z instead of z_0). Thus, $T_0(Z)$, $\alpha_0(Z)$, $\boldsymbol{\omega}_0(Z)$, $\mathbf{v}_0(Z)$, $q_0(Z)$, and $\beta_0(Z)$ are the environmental temperature, specific volume, vorticity, storm-relative wind, wind speed, and direction, respectively. The environmental variables provide upstream boundary conditions for the vorticity formulas that we develop. Henceforth we specify that the supercell is in the Northern Hemisphere. The environmental vorticity there is

$$\boldsymbol{\omega}_0 = -q_0 \frac{d\beta_0}{dZ}\mathbf{t}_0 + \frac{dq_0}{dZ}\mathbf{n}_0, \tag{23}$$

where $\mathbf{t}_0$ and $\mathbf{n}_0$ are unit horizontal vectors in and 90° to the left of the environmental wind direction, respectively, β_0 is the environmental wind direction measured counterclockwise from due east, $-q_0\, d\beta_0/dZ$ is the environmental streamwise vorticity (or minus the directional shear), and dq_0/dZ is the environmental transverse vorticity (or speed shear) (Davies-Jones 1984, hereafter DJ84).

Evaluation of the Bernoulli function $B(Z)$ in the upstream environment provides the formula

$$B(Z) = q_0^2/2 + c_p T_0 + gZ. \tag{24}$$

The environment is in hydrostatic equilibrium so

$$0 = T_0 \frac{dS}{dZ} - c_p \frac{dT_0}{dZ} - g. \tag{25}$$

We define the excess of a quantity as the local value of the quantity minus its value far upstream on the same Z surface. Let $T' \equiv T - T_0(Z)$ be the excess temperature. From (24) and (25),

$$\frac{dB}{dZ} = \frac{d}{dZ}\frac{q_0^2}{2} + T_0\frac{dS}{dZ} = T\frac{dS}{dZ} + \left(q_0\frac{dq_0}{dZ} - T'\frac{dS}{dZ}\right). \tag{26}$$

From (17) and (26),

$$Q^* = q_0\frac{dq_0}{dZ} - T'\frac{dS}{dZ}. \tag{27}$$

On a Z surface, we see that the constant barotropic part of Q^* is $Q^*_{\mathrm{BT}} = q_0\, dq_0/dZ$, and the variable baroclinic part is $Q^*_{\mathrm{BC}} = -T'dS/dZ$.

The segments of streamlines that lie in the undisturbed environment are horizontal straight lines parallel to the wind direction. We define right-handed coordinates (s, n_0, Z) where in each level of the environment s and n_0 are distances in and 90° to the left of the environmental wind direction, respectively. Note that in the veering environmental wind field s and n_0 vary with Z as follows: $ds/dZ = n_0\, d\beta_0/dZ$, $dn_0/dZ = -s\, d\beta_0/dZ$. The integral of (6) in the environment [where $a = 1$, $q = q_0$, and $\nabla Z = \mathbf{k}$ (the upward unit vector)] stipulates the environmental streamfunction

$$\psi = q_0 n_0. \tag{28}$$

The barotropic vortex lines also are straight in the environment. From (21) applied to the environment (where $\boldsymbol{\omega}_{\mathrm{BC}} = \mathbf{0}$) and (23),

$$\begin{aligned} \frac{\partial M_0}{\partial n_0} &= -q_0\frac{d\beta_0}{dZ}, \\ \frac{\partial M_0}{\partial s} &= -\frac{\partial q_0}{\partial Z}. \end{aligned} \tag{29}$$

Therefore,

$$M_0 = -\frac{dq_0}{dZ}s - q_0\frac{d\beta_0}{dZ}n_0 \tag{30}$$

is the equation for the barotropic vortex lines in the environment. A solution for M must approach M_0 far upstream.

Note that the excess temperature of a parcel is relative to its temperature far upstream where it is generally at a different height. Owing to compression (expansion), the excess temperature is positive (negative) in a downdraft (updraft). In contrast, warm updrafts and cool downdrafts are relative to the environmental temperature at the same level. They occur in the idealized flow only if the environment is absolutely unstable ($dS/dZ < 0$).

4. The Davies-Jones (2000) model

The DJ00 model uses the primary flow–secondary flow approach and the Boussinesq approximation. Let (x, y, z) be the customary Cartesian Eulerian coordinates, $\mathbf{u} \equiv (u, v, w)$ be the wind, and $\boldsymbol{\omega} \equiv (\xi, \eta, \zeta)$ be the vorticity in this system. The Lagrangian coordinates of the parcel that is at (x, y, z) at time τ are (X, Y, Z), its coordinates at a long-ago initial time τ_0 when it was far upstream. The primary flow consists of steady 3D potential flow (devoid of vorticity) with uniform velocity $(U, 0, 0)$ far upstream around a simple obstacle such as a sphere. There are three such objects for which an exact solution exists. DJ00 introduced environmental stratification $N^2 \equiv (g/c_p)\, dS/dZ$ and environmental vorticity $(-dV/dZ, dU/dZ, 0)$ as secondary effects without modifying the flow and calculated the resulting vorticity fields from analytical formulas. Here N^2 is the environmental Brunt–Väisälä frequency squared. Vertical displacement of isentropic surfaces that are horizontal in the far field (i.e., constant-Z surfaces) produces secondary baroclinity. The flow has zero PV so the vortex lines of the partial vorticities lie in the Z surfaces. DJ00 presented some results for stably stratified flow over the obstacle and applied the results to cyclonic and anticyclonic lee vortices. However, the model also applies to unstably stratified flow under the obstacle (see Fig. 5.12 in DJ+01), which is the relevant case for air subsiding in a negatively buoyant downdraft. Since there is secondary environmental vertical shear, we concentrate on a specific Z surface, let $h(x, y)$ be the surface's height and let $(U, 0, 0)$ be the upstream velocity on this surface. By (6) there exists a streamfunction $\psi(x,y)$ for the primary flow in this surface such that

$$\mathbf{u} = \frac{\partial Z}{\partial z}\left[\frac{\partial \psi}{\partial y}, -\frac{\partial \psi}{\partial x}, -\frac{\partial(\psi, h)}{\partial(x, y)}\right]. \tag{31}$$

As shown in sections 5 and 12 of DJ00, the secondary vorticity decomposes into three partial vorticities

$$\boldsymbol{\omega} = \boldsymbol{\omega}_{\mathrm{BTIS}} + \boldsymbol{\omega}_{\mathrm{BTIC}} + \boldsymbol{\omega}_{\mathrm{BC}}, \tag{32}$$

where on the Z surface

$$\boldsymbol{\omega}_{\mathrm{BTIS}} = -\frac{\partial Z}{\partial z}\frac{dV}{dZ}\left[\frac{\partial Y}{\partial y}, -\frac{\partial Y}{\partial x}, -\frac{\partial(Y, h)}{\partial(x, y)}\right] \tag{33}$$

is the barotropic vorticity arising from streamwise environmental vorticity $-dV/dZ$,

$$\boldsymbol{\omega}_{\mathrm{BTIC}} = \frac{\partial Z}{\partial z}\frac{dU}{dZ}\left[-\frac{\partial X}{\partial y}, \frac{\partial X}{\partial x}, \frac{\partial(X, h)}{\partial(x, y)}\right] \tag{34}$$

is the barotropic vorticity arising from crosswise environmental vorticity dU/dZ,

$$\boldsymbol{\omega}_{\mathrm{BC}} = \frac{\partial Z}{\partial z}\frac{dS}{dZ}\left[\frac{\partial \Lambda}{\partial y}, -\frac{\partial \Lambda}{\partial x}, -\frac{\partial(\Lambda, h)}{\partial(x, y)}\right] \tag{35}$$

is the baroclinic vorticity, and Λ is the cumulative temperature excess (the temporal integral following a parcel of its temperature minus its temperature far upstream). Note that all the partial vorticities increase inversely with the vertical spacing of the Z surfaces. The quantities $-Y dV/dZ$, $-X dU/dZ$, and $\Lambda dS/dZ$ serve as vortex-line functions for the partial vorticities. We find from conditions far upstream that $\psi = UY + \text{const}$. Hence $\boldsymbol{\omega}_{\mathrm{BTIS}} = (-dV/dZ)\,\mathbf{u}/U$ and its vortex-line function is $(-dV/dZ)\,\psi/U$. Thus the vortex lines of $\boldsymbol{\omega}_{\mathrm{BTB}}$ coincide with the streamlines, and $\boldsymbol{\omega}_{\mathrm{BTIS}}$ is a Beltrami vorticity in the steady flow.

As illustrations of the general theory's geometric constructs (Z surfaces, vortex lines) and the vorticity decomposition, we present computer plots generated by the DJ00 model. Figure 1 depicts in 3D a constant-Z surface for flow under a sphere. The parcels in this surface descend in a shallow divergent downdraft and then ascend in a shallow convergent updraft. Figure 2 shows the contours of surface height, vertical vorticity, and vortex-line function for environmental wind $U = 10\,\mathrm{m\,s^{-1}}$, environmental streamwise vorticity $-dV/dZ = 1 \times 10^{-2}\,\mathrm{s^{-1}}$, environmental crosswise vorticity $dU/dZ = 7 \times 10^{-3}\,\mathrm{s^{-1}}$, and unstable environmental stratification with $N^2 = -10^{-4}\,\mathrm{s^{-2}}$. The Richardson number $\mathrm{Ri} \equiv N^2/[(dU/dZ)^2 + (dV/dZ)^2]$ is -0.8, which indicates that helical and buoyancy effects are comparable (Kanak and Lilly 1996). The streamlines of the primary flow are the long dashed lines in Fig. 3. The full vorticity field in Fig. 2 consists of the three partial-vorticity fields.

The first partial vorticity is the Beltrami barotropic one $\boldsymbol{\omega}_{\mathrm{BTIS}}$, which depends just on the streamwise environmental vorticity $-dV/dZ$ (with dU/dZ and N^2 set to zero for its computation). Its vortex lines coincide with the streamlines and contours of its vertical component coincide with the contours of vertical velocity (Fig. 3). The maximum vertical velocity is $5\,\mathrm{m\,s^{-1}}$. For the above

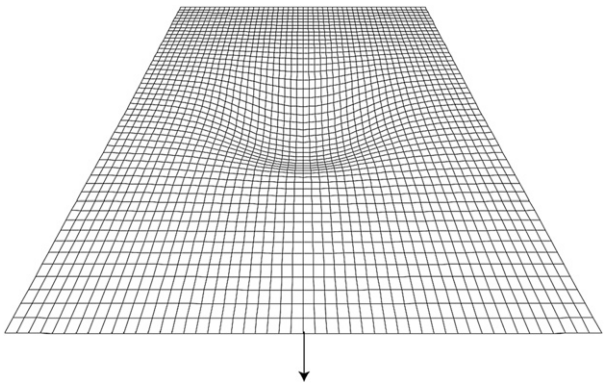

FIG. 1. 3D ''chickenwire'' diagram of a specific Z surface for flow under a sphere of radius 1 km. The arrow indicates the predominant flow direction. At infinity and the nadir the surface is lower than the height of the sphere's centroid by 0.5 and 1.08 km, respectively.

environmental wind parameters, $\boldsymbol{\omega}_{\mathrm{BTIS}} = 10^{-3}\,\mathbf{u}$ and the maximum value of ζ_{BTIS} is $5 \times 10^{-3}\,\mathrm{s}^{-1}$. The ζ_{BTIS} field features an upstream anticyclonic vortex and downstream cyclonic vortex with zero ζ_{BTIS} at the nadirs of the streamlines. This is agreement with Fig. 16b in Markowski et al. (2008, hereafter M+08).

The second partial vorticity is the barotropic one owing to imported storm-relative crosswise vorticity $\boldsymbol{\omega}_{\mathrm{BTIC}}$, which depends just on the speed shear dU/dZ. Its vortex-line function and vertical component are contoured in Fig. 4. The vortex lines of $\boldsymbol{\omega}_{\mathrm{BTIC}}$ are transverse far upstream and are frozen in the flow. As the flow slows and turns to go around the obstacle, these vortex lines are held back in front of the obstacle and bent as shown, producing streamwise (antistreamwise) vorticity on the left (right) side of the flow through the river-bend effect. The vortex pair in the ζ_{BTIC} field is slightly in the lee of the sphere with the cyclonic (anticyclonic) vortex on the left (right) side as depicted in Fig. 9 (top) of DJB93.

Now consider baroclinity effects. In unstably stratified flow under the sphere, baroclinic vorticity is generated in the form of horizontal rings with the vorticity directed clockwise around the rings when viewed from above. Consider one such ring that is generated in one infinitesimal time interval around one height contour of its depressed parent Z surface. It is deformed and advected downstream by the primary flow. In other words, it is frozen in the flow after generation. Because the leading (trailing) edge is initially in updraft (downdraft), advection tilts the ring, causing cyclonic (anticyclonic) vorticity on the left (right) side of the flow. Figure 5 shows the baroclinic-vorticity field produced by vorticity generation during the previous 5 min. It is the net result of all rings generated around every contour in every subinterval of the 5-min window after transport to the present time by the frozen-in-flow mechanism. The resultant baroclinic vortex lines are tilted closed loops, which become elongated as a result of a stationary generation region and downstream advection. This vortex-line structure and evolution is similar to the depictions in M+08 (see their Figs. 17 and 19).

The steady baroclinic vorticity $\boldsymbol{\omega}_{\mathrm{BC}}$ is the third partial vorticity. It has vortex lines that are shaped like hairpins (Fig. 6). The legs of the hairpins stem from vorticity generated a while ago and subsequently advected downstream whereas the heads originate from vorticity generated very recently. At the surface's nadir, $\partial Z/\partial z = 3$ and the local stratification is thus 3 times greater than the environmental value. The baroclinic vortex lines cross the streamlines so in steady flow the baroclinic vorticity has a significant crosswise component as well as a streamwise one (also deduced by Dahl 2015). There is nonzero ζ_{BC} at the nadirs of the streamlines except for the central one (DJB93; DJ00). The vortex pair in the ζ_{BC} field has the same orientation as the one in the ζ_{BTIC} field, but it is located farther downstream. Scale analysis indicates the baroclinic vorticity increases with greater unstable stratification; longer, narrower, or deeper baroclinic zone; or slower parcel speed through the zone (DJ+01, 183–184).

The values of environmental stratification and vorticity were chosen so that the vertical components of each partial vorticity have the same maximum and minimum values ($\pm 5 \times 10^{-3}\,\mathrm{s}^{-1}$). The vorticity field in Fig. 2 is the sum of the ones in Figs. 3, 4, and 6. The downstream location and transverse orientation of the vortex pair in the $\boldsymbol{\omega}_{\mathrm{BTIC}}$ and $\boldsymbol{\omega}_{\mathrm{BC}}$ fields (Figs. 4 and 6) together with the streamwise orientation of the vortex pair in the $\boldsymbol{\omega}_{\mathrm{BTIS}}$ field across the nadir of the Z surface (Fig. 3) results in a stronger cyclonic vortex in updraft on the left downstream side and a weaker anticyclonic one in near-zero vertical velocity on the right side in Fig. 2.

We can model also updraft rotation by unstably stratified flow over the sphere. The same diagrams apply except the signs of h, Λ, w, ξ_{BC}, η_{BC}, and ζ_{BT} are reversed. In this case the vortex lines of $\boldsymbol{\omega}_{\mathrm{BTIC}}$ and $\boldsymbol{\omega}_{\mathrm{BTIS}}$ match the depictions in Figs. 7 and 8 of DJ84.

In the next sections we develop improved theory that abandons the primary–secondary flow approach and thus eliminates the assumption of primary flow that is essentially straight, low speed, and irrotational.

5. Natural coordinates

Because the streamlines and vortex lines are contained in the Z surfaces, we can solve for vorticity in

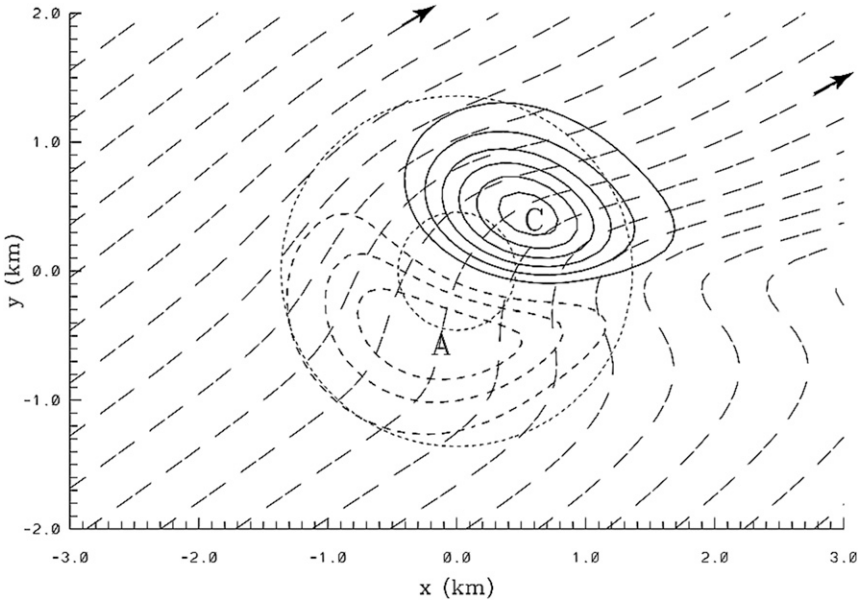

FIG. 2. Vortex lines of $\boldsymbol{\omega}$ and contours of vertical vorticity ζ in the Z surface of Fig. 1 for an environmental wind U of 10 m s^{-1} in the x direction, environmental streamwise vorticity of 1×10^{-2} s^{-1}, environmental crosswise vorticity of 7×10^{-3} s^{-1}, and $N^2 = -10^{-4}$ s^{-2}. The dotted circles are the -600 and -1000 height contours of the Z surface. The long dashed unclosed lines are contours of the vortex-line function with contour interval (CI) of 4 m s^{-1} and arrows on a few to indicate the direction of vorticity. C and A mark the locations of the maximum and minimum values (-0.008 and $+0.013$ s^{-1}) of ζ. The ζ field is contoured at intervals of 0.002 s^{-1} with the zero contour omitted. The closed solid lines around C are the positive contours of ζ, and the closed dashed lines around A are the negative contours.

each surface independently. In a particular Z surface, say Σ, we use a right-handed orthonormal natural basis system with unit vectors **t**, **n**, and **b**, where **t** is in the flow direction, **n** is tangential to Σ and 90° to the left of the flow, and $\mathbf{b} \equiv \mathbf{t} \times \mathbf{n} \equiv \nabla Z/|\nabla Z|$ is normal to Σ (Fig. 3). We call the directions of **t**, **n**, and **b** the streamwise, transverse, and binormal directions, respectively, the curves in Σ that are perpendicular to the streamlines the transverses, and the curves that are perpendicular to the Z surfaces the binormals. Recall that in this paper "streamwise" means parallel to the three-directional wind $\mathbf{v} = q\mathbf{t}$, where q is the wind speed. The elements of arclength along streamlines, transverses, and binormals—ds, dn and db, respectively—define a natural coordinate system. We also use a semi-Lagrangian natural coordinate system (s, n_0, Z) with the basis vectors **t**, **n**, and **b**. A given point P in Σ is identified first by Z, the height of Σ in the environment; next by n_0, which is a linear function of ψ through (28) and hence labels the streamline through P; and finally by s, the arclength along the streamline. All integrals below are along a streamline (with n_0 and Z held constant). In Σ, we assume that the locus of $s = 0$ is along a straight transverse in the far environment and that variables take on their environmental values on and upstream of this line with only insignificant loss of accuracy. In this way we avoid improper integrals with limits of $-\infty$ and use the same curve parameter for all the streamlines in Σ. Note that the curves of constant s in Σ are orthogonal to the streamlines only in the environment. In the language of first-order partial differential equations (Farlow 1993, 206–207), $s = 0$ is the initial curve and the streamlines are the characteristics. A formula for transverse vorticity is obtained easily from Crocco's theorem. Terms involving transverse vorticity and baroclinity act as forcing terms in the streamwise-vorticity equation. The solution for streamwise vorticity is constructed by integrating first-order ordinary differential equations along the characteristics with the environmental sounding providing the starting conditions. This paper focuses on the variation of vorticity along an individual streamline.

The vorticity vector in zero-PV flow is $\boldsymbol{\omega} = \omega_1\mathbf{t} + \omega_2\mathbf{n}$, where ω_1 and ω_2 are the three-directional streamwise and transverse components of vorticity. The entropy equation and the constraint of zero PV are satisfied in the natural system by $\mathbf{t} \cdot \nabla Z = \mathbf{n} \cdot \nabla Z = 0$. Thus, $\nabla Z = (dZ/db)\,\mathbf{b}$, where dZ/db is the inverse of db/dZ and db

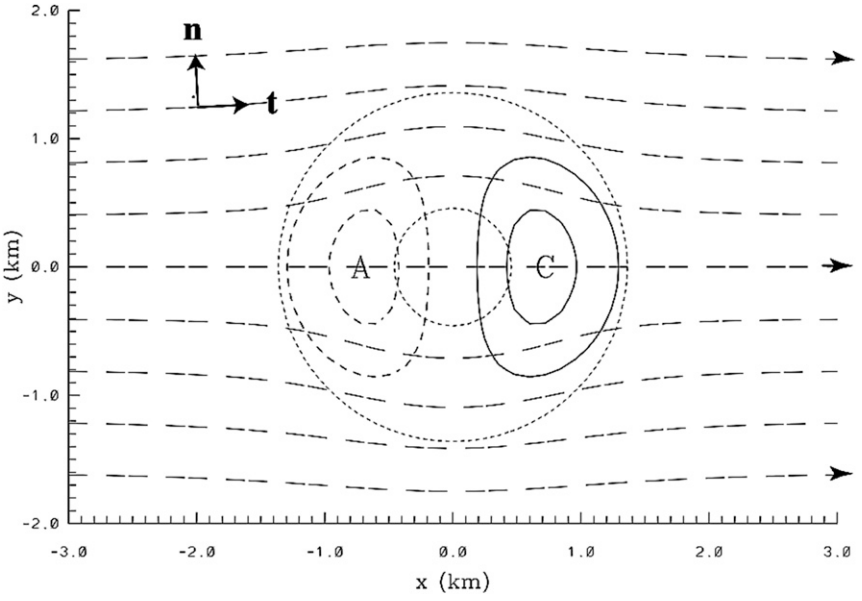

FIG. 3. As in Fig. 2, but for the (Beltrami) barotropic partial vorticity arising from imported storm-relative streamwise vorticity $\boldsymbol{\omega}_{\mathrm{BTIS}}$ instead of the full vorticity $\boldsymbol{\omega}$. In this figure only, the long dashed lines are the primary flow's streamlines as well as the vortex lines of $\boldsymbol{\omega}_{\mathrm{BTIS}}$, and the closed contours around A and C are contours of the primary vertical velocity w as well as of ζ_{BTIS}. The CIs of the streamfunction and w are $4000\,\mathrm{m^2\,s^{-1}}$ and $2\,\mathrm{m\,s^{-1}}$, respectively. Also included are **t** and **n,** the streamwise and transverse unit vectors at a point. The binormal unit vector **b** at this point is the upward normal to the surface.

is the distance along a binormal curve between two surfaces with an environmental height difference of dZ. Since $B = B(Z)$, Crocco's theorem (1) becomes

$$-q\omega_2\mathbf{b} = \left(T\frac{dS}{dZ} - \frac{dB}{dZ}\right)\frac{dZ}{db}\mathbf{b}. \tag{36}$$

The streamfunction definition [(6)] produces

$$\frac{\partial\psi}{\partial n} = \frac{q}{a}\frac{db}{dZ}. \tag{37}$$

We adopt some special notation to avoid pitfalls that might arise because the constant-s curves are oblique to the streamlines. In this paper, ϕ denotes a general scalar. By $\partial\phi/\partial s$ we mean $\mathbf{t}\cdot\nabla\phi$ or $(\partial\phi/\partial s)_{\psi,Z}$. Similarly, $\partial\phi/\partial b$ denotes $\mathbf{b}\cdot\nabla\phi = (\partial\phi/\partial b)_{s,\psi} = (\partial\phi/\partial Z)_{s,\psi}\ dZ/db$. Since $\mathbf{n}\cdot\nabla\phi$ is not generally equal to $(\partial\phi/\partial n)_{s,Z}$, the partial derivative of ϕ with s and Z held constant, we use the notation $\delta_\perp\phi/\delta_\perp n$ for $\mathbf{n}\cdot\nabla\phi$. The subscript $\perp$ indicates that the infinitesimal increment is taken along a transverse instead of along a curve of constant s. The two types of normal derivatives are different with a few exceptions since

$$\mathbf{n}\cdot\nabla\phi \equiv \frac{\delta_\perp\phi}{\delta_\perp n} = \left(\frac{\partial\phi}{\partial n}\right)_{s,Z} + \left(\frac{\partial\phi}{\partial s}\right)_{n,Z}\frac{\delta_\perp s}{\delta_\perp n}. \tag{38}$$

The last term arises from the change $\delta_\perp s$ in the streamline curve parameters in a transversal distance $\delta_\perp n$.

One exception is $\phi = n_0$. By taking $\partial/\partial s$ of (28) we obtain

$$\mathbf{t}\cdot\nabla n_0 \equiv \frac{\partial n_0}{\partial s} = 0, \tag{39}$$

since $\partial\psi/\partial s = 0$ and $n_0 = n_0(\psi)$. Consequently,

$$\mathbf{n}\cdot\nabla n_0 \equiv \frac{\delta_\perp n_0}{\delta_\perp n} = \left(\frac{\partial n_0}{\partial n}\right)_Z \equiv R, \tag{40}$$

where $R > 0$ is the ratio of the environmental streamline spacing $\delta_\perp n_0$ to the local spacing $\delta_\perp n$. By the chain rule, (28), and (37),

$$R = \frac{\partial n_0}{\partial\psi}\frac{\partial\psi}{\partial n} = \frac{q}{aq_0}\frac{db}{dZ}. \tag{41}$$

The inverse of (41) is

$$\frac{1}{R} = \frac{\delta_\perp n}{\delta_\perp n_0} = \frac{aq_0}{q}\frac{dZ}{db}. \tag{42}$$

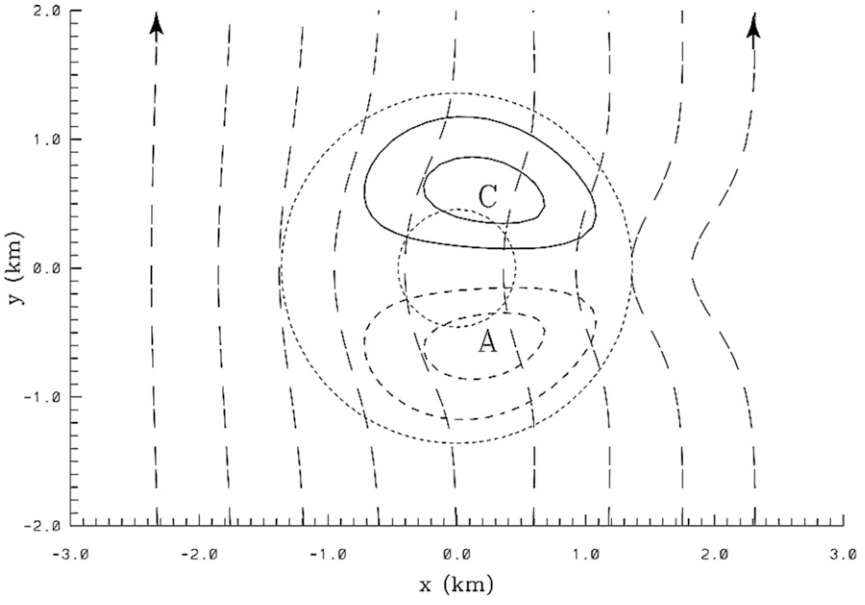

FIG. 4. As in Fig. 2, but for the barotropic partial vorticity arising from imported storm-relative crosswise vorticity $\boldsymbol{\omega}_{\mathrm{BTIC}}$.

By the chain rule,

$$\frac{\delta_\perp}{\delta_\perp n} = R\frac{\delta_\perp}{\delta_\perp n_0}. \tag{43}$$

We will also need $\mathbf{t}\cdot\nabla s_0$. The trajectory of a parcel along its streamline is described by $s(\tau)$, where τ is time in Lagrangian coordinates. At the current time τ, consider two adjacent parcels A and B on the same streamline at locations s and $s-\delta s$. Let τ be large so that, at time zero, A and B are in the environment at s_0 (<0) and $s_0-\delta s_0$, respectively. In time τ, A moves from s_0 to s and B moves from $s_0-\delta s_0$ to $s-\delta s$. Therefore,

$$\tau = \int_{s_0}^{s}\frac{1}{q(\sigma)}d\sigma = \int_{s_0-\delta s_0}^{s-\delta s}\frac{1}{q(\sigma)}d\sigma. \tag{44}$$

Subtracting one integral from the other and cancelling the parts in common yields

$$0 = \int_{s-\delta s}^{s}\frac{1}{q(\sigma)}d\sigma - \int_{s_0-\delta s_0}^{s_0}\frac{1}{q(\sigma)}d\sigma \Rightarrow \frac{\delta s}{q} = \frac{\delta s_0}{q_0}$$
$$\Rightarrow \mathbf{t}\cdot\nabla s_0 = \left(\frac{\partial s_0}{\partial s}\right)_{n_0,Z} = \frac{q_0}{q} \quad \text{and} \quad \left(\frac{\partial s}{\partial s_0}\right)_{n_0,Z} = \frac{q}{q_0}. \tag{45}$$

Thus, the separation AB is proportional to the wind speed.

We summarize the above relationships in the matrix equation

$$\begin{bmatrix}\nabla s_0\\ \nabla n_0\\ \nabla Z\end{bmatrix}\cdot[\mathbf{t}\quad\mathbf{n}\quad\mathbf{b}] = \begin{bmatrix}\partial s_0/\partial s & \cdots & \cdots\\ 0 & \partial n_0/\partial n & \cdots\\ 0 & 0 & dZ/db\end{bmatrix}$$
$$= \begin{bmatrix}q_0/q & \cdots & \cdots\\ 0 & \dfrac{q}{aq_0}\dfrac{db}{dZ} & \cdots\\ 0 & 0 & dZ/db\end{bmatrix}, \tag{46}$$

where the ellipses signify elements that are difficult to derive and not used below. From equality of the determinants in (46) we obtain the Lagrangian continuity equation

$$\frac{\partial s_0}{\partial s}\frac{\partial n_0}{\partial n}\frac{dZ}{db} = \frac{1}{a}, \tag{47}$$

which is equivalent to (42) since $\partial n_0/\partial n \equiv R$ and $\partial s_0/\partial s = q_0/q$.

Frenet's formulas (Mathews and Walker 1965) provide the variations of the unit vectors along a streamline. They are

$$\frac{\partial \mathbf{t}}{\partial s} = \kappa\mathbf{n},$$
$$\frac{\partial \mathbf{n}}{\partial s} = -\kappa\mathbf{t} - \gamma\mathbf{b}, \tag{48}$$
$$\frac{\partial \mathbf{b}}{\partial s} = \gamma\mathbf{n},$$

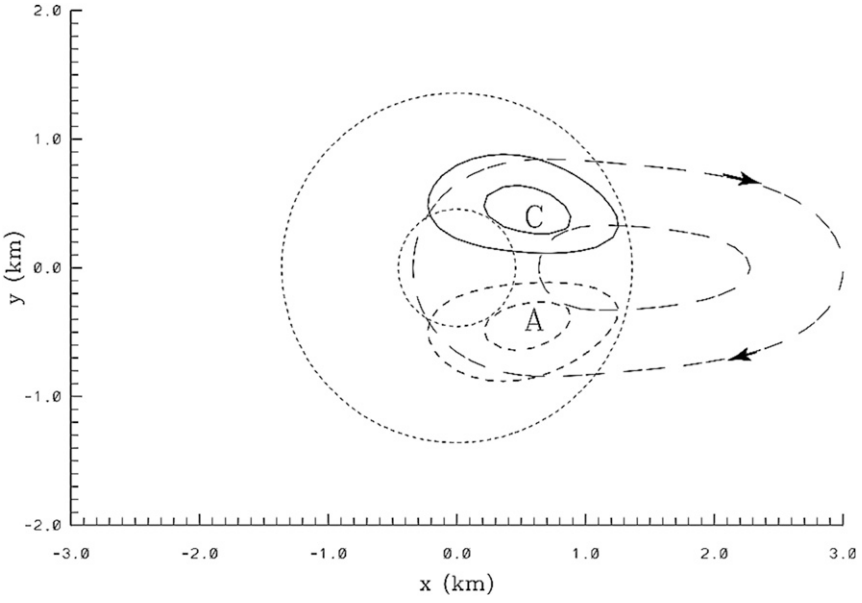

FIG. 5. As in Fig. 2, except for only the baroclinic vorticity generated during the previous 5 min and carried forward to the present by the primary flow. Over a finite time interval, the baroclinic vortex lines are elongated rings (long dashed lines).

where κ and γ are the curvature and torsion of the streamline. By taking $\partial/\partial r$ of $\mathbf{t}\cdot\mathbf{t}=1$, $\mathbf{t}\cdot\mathbf{n}=0$, and $\mathbf{t}\cdot\mathbf{b}=0$ where $\partial/\partial r$ is $\partial/\partial s$, $\delta_\perp/\delta_\perp n$, or $\partial/\partial b$, we find that

$$\begin{aligned}
&\mathbf{t}\cdot\frac{\partial\mathbf{t}}{\partial r}=0,\\
&\frac{\partial\mathbf{t}}{\partial r}\cdot\mathbf{n}=-\mathbf{t}\cdot\frac{\partial\mathbf{n}}{\partial r},\\
&\frac{\partial\mathbf{t}}{\partial r}\cdot\mathbf{b}=-\mathbf{t}\cdot\frac{\partial\mathbf{b}}{\partial r}.
\end{aligned}\tag{49}$$

We need the vorticity components in natural coordinates. The gradient vector operator is

$$\nabla\equiv\mathbf{t}\frac{\partial}{\partial s}+\mathbf{n}\frac{\delta_\perp}{\delta_\perp n}+\mathbf{b}\frac{\partial}{\partial b}.\tag{50}$$

The vorticity is therefore

$$\begin{aligned}
\boldsymbol{\omega}&=\nabla\times(q\mathbf{t})=\nabla q\times\mathbf{t}+q\left(\mathbf{t}\frac{\partial}{\partial s}+\mathbf{n}\frac{\delta_\perp}{\delta_\perp n}+\mathbf{b}\frac{\partial}{\partial b}\right)\times\mathbf{t}\\
&=\frac{\delta_\perp q}{\delta_\perp n}\mathbf{n}\times\mathbf{t}+\frac{\partial q}{\partial b}\mathbf{b}\times\mathbf{t}\\
&\quad+q\left(\mathbf{t}\times\frac{\partial\mathbf{t}}{\partial s}+\mathbf{n}\times\frac{\delta_\perp\mathbf{t}}{\delta_\perp n}+\mathbf{b}\times\frac{\partial\mathbf{t}}{\partial b}\right).
\end{aligned}\tag{51}$$

Via (48), (49), and (14), we obtain

$$\begin{aligned}
\boldsymbol{\omega}&=-\frac{\delta_\perp q}{\delta_\perp n}\mathbf{b}+\frac{\partial q}{\partial b}\mathbf{n}\\
&\quad+q\left[\mathbf{t}\times\frac{\partial\mathbf{t}}{\partial s}-\frac{\delta_\perp\mathbf{t}}{\delta_\perp n}\times(\mathbf{b}\times\mathbf{t})-\frac{\partial\mathbf{t}}{\partial b}\times(\mathbf{t}\times\mathbf{n})\right]\\
&=-\frac{\delta_\perp q}{\delta_\perp n}\mathbf{b}+\frac{\partial q}{\partial b}\mathbf{n}+q\left[\kappa\mathbf{b}+\left(\frac{\delta_\perp\mathbf{t}}{\delta_\perp n}\cdot\mathbf{b}\right)\mathbf{t}-\left(\frac{\partial\mathbf{t}}{\partial b}\cdot\mathbf{n}\right)\mathbf{t}\right]\\
&=\left[q\mathbf{t}\cdot\left(\frac{\partial\mathbf{n}}{\partial b}-\frac{\delta_\perp\mathbf{b}}{\delta_\perp n}\right)\right]\mathbf{t}+\frac{\partial q}{\partial b}\mathbf{n}+\left(\kappa q-\frac{\delta_\perp q}{\delta_\perp n}\right)\mathbf{b}.
\end{aligned}\tag{52}$$

The expression for streamwise vorticity contained in (52) is impractical, but the transverse vorticity is simply $\mathbf{b}\cdot\nabla q$, the directional derivative of the wind speed gradient in the binormal direction. For a zero-PV flow there is no vorticity normal to the Z surfaces; hence, by (43),

$$\frac{\delta_\perp q}{\delta_\perp n}=\kappa q\quad\Rightarrow\quad\kappa=\frac{\delta_\perp\ln q}{\delta_\perp n}=R\frac{\delta_\perp\ln q}{\delta_\perp n_0}.\tag{53}$$

6. The transverse vorticity

The transverse vorticity ω_2 is obtained directly from Crocco's theorem [(1)]. It is related to the Lamb vector $\mathbf{L}\equiv\boldsymbol{\omega}\times\mathbf{v}$ by

$$\omega_2\equiv\boldsymbol{\omega}\cdot\mathbf{n}=\boldsymbol{\omega}\cdot(\mathbf{b}\times\mathbf{t})=-\frac{1}{q}\mathbf{b}\cdot(\boldsymbol{\omega}\times\mathbf{v})\tag{54}$$

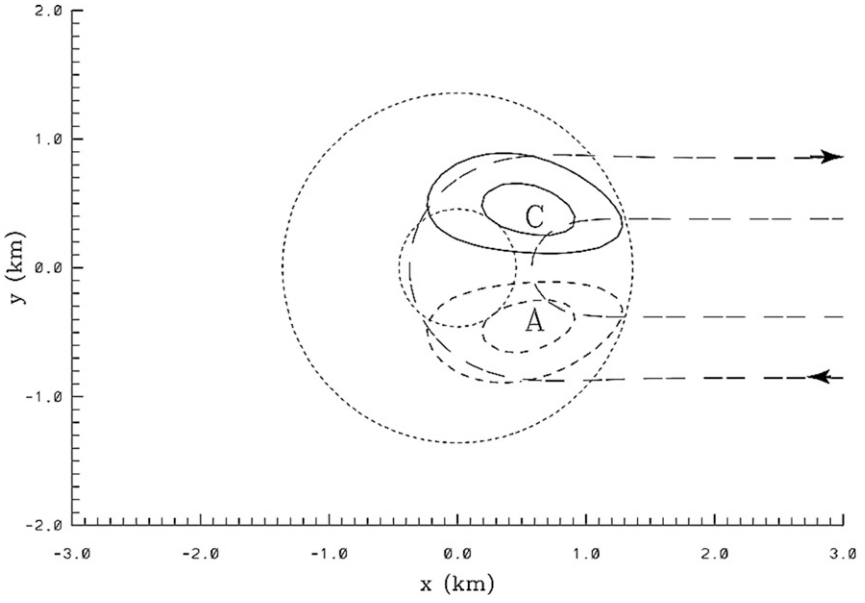

FIG. 6. As in Fig. 5, but for the steady baroclinic partial-vorticity field $\boldsymbol{\omega}_{\mathrm{BC}}$. In infinite time, the baroclinic vortex lines become hairpins (long dashed unclosed lines).

(Scorer 1997, p. 78). From (20) and (27),

$$\mathbf{L} = -Q^*\nabla Z = \left(T'\frac{dS}{dZ} - q_0\frac{dq_0}{dZ}\right)\nabla Z. \tag{55}$$

Substituting for $\mathbf{L}$ in (54) then yields

$$\omega_2 \equiv \frac{\partial q}{\partial b} = \frac{Q^*}{q}\frac{dZ}{db} = \frac{q_0}{q}\frac{dq_0}{dZ}\frac{dZ}{db} - \frac{T'}{q}\frac{dS}{dZ}\frac{dZ}{db}, \tag{56}$$

where the terms involving dq_0/dz and dS/dZ are the transverse barotropic vorticity and transverse baroclinic vorticity, respectively. These terms satisfy the upstream boundary conditions $\boldsymbol{\omega}_{\mathrm{BT}}\cdot\mathbf{n} = dq_0/dZ$, $\boldsymbol{\omega}_{\mathrm{BC}}\cdot\mathbf{n} = 0$ at $s \le 0$. Multiplying (56) by a and substituting for $(a/q\, dZ/db)$ from (42) gives the useful formula

$$a\omega_2 = \frac{Q^*}{q_0 R}. \tag{57}$$

7. The vector vorticity equation in natural coordinates

In contrast to the transverse vorticity ω_2 that follows from Crocco's theorem, we can obtain the streamwise vorticity ω_1 only by solving the vector vorticity equation [(8)]. Although we know ω_2 and $\boldsymbol{\omega}\cdot\mathbf{b}$ is zero here, we still have to use the transverse and binormal vorticity equations because they determine the vector $\delta_\perp\mathbf{t}/\delta_\perp n$. We require $\delta_\perp\mathbf{t}/\delta_\perp n$ to find a formula for the commutator

$$\frac{\delta_\perp}{\delta_\perp n}\left(\frac{\partial\phi}{\partial s}\right) - \frac{\partial}{\partial s}\left(\frac{\delta_\perp\phi}{\delta_\perp n}\right).$$

In turn, we need this commutator to obtain the streamwise-vorticity solution.

In natural coordinates, (8) becomes

$$q\frac{\partial}{\partial s}(a\omega_1\mathbf{t} + a\omega_2\mathbf{n}) - \left(a\omega_1\frac{\partial}{\partial s} + a\omega_2\frac{\delta_\perp}{\delta_\perp n}\right)(q\mathbf{t}) = a\frac{\delta_\perp T'}{\delta_\perp n}\frac{dS}{db}\mathbf{t} - a\frac{\partial T'}{\partial s}\frac{dS}{db}\mathbf{n}. \tag{58}$$

After dividing both sides by q^2 and some manipulations, we obtain

$$\frac{\partial}{\partial s}\left(\frac{a\omega_1\mathbf{t} + a\omega_2\mathbf{n}}{q}\right) + \frac{a\omega_2}{q}\frac{\partial \ln q}{\partial s}\mathbf{n} - \frac{a\omega_1}{q}\frac{\partial\mathbf{t}}{\partial s} - \frac{a\omega_2}{q}\left(\frac{\delta_\perp\mathbf{t}}{\delta_\perp n} + \frac{\delta_\perp \ln q}{\delta_\perp n}\mathbf{t}\right) = \frac{a}{q^2}\frac{dS}{db}\left(\frac{\delta_\perp T'}{\delta_\perp n}\mathbf{t} - \frac{\partial T'}{\partial s}\mathbf{n}\right). \tag{59}$$

Via (53) and Frenet's equation [(48)] we get

$$\frac{\partial}{\partial s}\left(\frac{a\omega_1}{q}\right)\mathbf{t} + \frac{1}{q}\frac{\partial}{\partial s}(a\omega_2)\mathbf{n} - \frac{a\omega_2}{q}(\kappa\mathbf{t} + \gamma\mathbf{b}) - \frac{a\omega_2}{q}\frac{\delta_\perp\mathbf{t}}{\delta_\perp n} - \frac{a\omega_2}{q}\kappa\mathbf{t} = \frac{a}{q^2}\frac{dS}{db}\left(\frac{\delta_\perp T'}{\delta_\perp n}\mathbf{t} - \frac{\partial T'}{\partial s}\mathbf{n}\right). \tag{60}$$

The scalar product of (60) with **b** tells us that

$$\frac{\delta_\perp \mathbf{t}}{\delta_\perp n}\cdot\mathbf{b} = -\gamma \tag{61}$$

when $\omega_2 \neq 0$. The dot product of (60) with **n** times q^2/a yields

$$\frac{q}{a}\frac{\partial}{\partial s}(a\omega_2) - q\omega_2\frac{\delta_\perp \mathbf{t}}{\delta_\perp n}\cdot\mathbf{n} = -\frac{\partial T'}{\partial s}\frac{dS}{dZ}\frac{dZ}{db} \equiv G_2, \tag{62}$$

where $\mathbf{G} \equiv G_1\mathbf{t} + G_2\mathbf{n} \equiv \nabla T \times \nabla S$ is the baroclinic generation term in the vorticity equation. From (57) $a\omega_2 = Q^*/q_0R$, from (42) $(a/q)\,dZ/db = 1/q_0R$, and from (27) $\partial Q^*/\partial s = -\partial T'/\partial s\; dS/dZ$. Therefore,

$$Q^*\left(\frac{1}{R}\frac{\partial R}{\partial s} + \frac{\delta_\perp \mathbf{t}}{\delta_\perp n}\cdot\mathbf{n}\right) = 0. \tag{63}$$

Hence, by (49), (63), and (61),

$$\frac{\delta_\perp \mathbf{t}}{\delta_\perp n} = -\frac{1}{R}\frac{\partial R}{\partial s}\mathbf{n} - \gamma\mathbf{b} \tag{64}$$

if $Q^* \neq 0$ (if $Q^* = 0$, $\omega_2 = 0$). After use of (64), multiplication by Ra/q, and integration along a streamline (with n_0 and Z held constant and suppressed in the function arguments), we get

$$\omega_2(s) = \Psi(s,0)\omega_2(0) + \int_{\sigma=0}^{s}\Psi(s,\sigma)G_2(\sigma)\frac{d\sigma}{q(\sigma)}, \quad \Psi(s,\sigma) \equiv \frac{R(\sigma)a(\sigma)}{R(s)a(s)}, \tag{65}$$

with the far-upstream conditions $R(0) = a(0) = 1$, $\omega_2(0) = dq_0/dZ$. Reassuringly, substituting for Ra from (41) into (65) recovers (56). In (65) $d\sigma/q(\sigma) \equiv d\tau$ is the Lagrangian element of time and $G_2(\sigma)\,d\tau$ is a parcel's incremental gain of baroclinic transverse vorticity owing to its presence in a streamwise temperature gradient. The term $\Psi(s,\sigma)$ is the propagator for transverse vorticity. It propagates the environmental ω_2 of a parcel forward in time to the present, and from their generation times it projects forward the increments of baroclinic transverse vorticity; Ψ modulates the individual contributions with the ratio of the streamline spacing at the generation or initial time to the current spacing.

The scalar product of (60) with **t** and use of (49) yields the streamwise-vorticity equation

$$\frac{q^2}{a}\frac{\partial}{\partial s}\left(\frac{a\omega_1}{q}\right) = 2\kappa q\omega_2 + \frac{\delta_\perp T'}{\delta_\perp n}\frac{dS}{db} \equiv K + G_1, \tag{66}$$

where $K \equiv 2\kappa q\omega_2$ is the curvature forcing term. This is a generalization of the equation derived by Scorer (1997, p. 81). The integral of (66) is

$$\omega_1(s) = \Phi(s,0)\omega_1(0) + \int_{\sigma=0}^{s}\Phi(s,\sigma)[K(\sigma) + G_1(\sigma)]\frac{d\sigma}{q(\sigma)},$$
$$\Phi(s,\sigma) \equiv \frac{q(s)a(\sigma)}{q(\sigma)a(s)}, \tag{67}$$

where $\Phi(s,\sigma)$ is the propagator for streamwise vorticity.

We discuss (67) later and meanwhile search for a more useful formula for streamwise vorticity. From (21) and (50) χ is related to the vorticity components by

$$\omega_1 = \frac{\delta_\perp \chi}{\delta_\perp n}\frac{dZ}{db}, \quad \omega_2 = -\frac{\partial \chi}{\partial s}\frac{dZ}{db}. \tag{68}$$

After substituting for ω_1 and ω_2 from (68) and for $(a/q)\,dZ/db$ from (42), (66) becomes

$$\frac{\partial}{\partial s}\left(\frac{1}{R}\frac{\delta_\perp \chi}{\delta_\perp n}\right) = \frac{1}{R}\left(-2\kappa\frac{\partial \chi}{\partial s} + \frac{1}{q}\frac{\delta_\perp T'}{\delta_\perp n}\frac{dS}{dZ}\right). \tag{69}$$

Via (43) and (53), this converts to

$$\frac{\partial}{\partial s}\left(\frac{\delta_\perp \chi}{\delta_\perp n_0}\right) = -\frac{2}{q}\frac{\delta_\perp q}{\delta_\perp n_0}\frac{\partial \chi}{\partial s} + \frac{1}{q}\frac{\delta_\perp T'}{\delta_\perp n_0}\frac{dS}{dZ} \tag{70}$$

in (s, n_0, Z) coordinates.

8. Integral of the vector vorticity equation

We obtain a formula for the streamwise vorticity by integrating (70) and imposing the upstream boundary conditions on $\boldsymbol{\omega}_{\mathrm{BC}}$ and $\boldsymbol{\omega}_{\mathrm{BT}}$. Applying the commutation relation [(B6)] and multiplying both sides by q yields

$$\frac{\delta_\perp}{\delta_\perp n_0}\left(q\frac{\partial \chi}{\partial s} - T'\frac{dS}{dZ}\right) = 0. \tag{71}$$

Since $\Lambda = 0$ at $s \leq 0$, the upstream boundary condition on χ ($\equiv M + \Lambda\, dS/dZ$) is

$$\chi(s, n_0, Z) = -\frac{dq_0}{dZ}s - q_0\frac{d\beta_0}{dZ}n_0, \quad \forall s \leq 0 \tag{72}$$

from (30). The boundary condition at lateral infinity where the environment is undisturbed is

$$\frac{\partial \chi}{\partial s} \to -\frac{dq_0}{dZ}, \quad q \to q_0, \quad T' \to 0 \quad \text{as} \quad |n_0| \to \infty \tag{73}$$

from (30) again. Integrating (71) with respect to n_0 along a transverse gives

$$q\frac{\partial\chi}{\partial s} = T'\frac{dS}{dZ} + F(s,Z), \tag{74}$$

where $F(s, Z)$ is a function of integration equal to $-q_0\, dq_0/dZ$ because of (73). Thus, (74) becomes

$$\frac{\partial\chi}{\partial s} = \frac{T'}{q}\frac{dS}{dZ} - \frac{q_0}{q}\frac{dq_0}{dZ} = -\frac{Q^*}{q} \tag{75}$$

by (27). The integral of (75) with respect to s that satisfies the upstream boundary condition [(72)] at $s = 0$ is

$$\chi(s,n_0,Z) = -q_0\frac{d\beta_0}{dZ}n_0 - \int_{\sigma=0}^{s}\frac{Q^*(\sigma,n_0,Z)}{q(\sigma,n_0,Z)}d\sigma, \tag{76}$$

where $Q^* = q_0\, dq_0/dZ - T'dS/dZ$ from (27). In summary, the vorticity is

$$\boldsymbol{\omega} = \nabla\chi\times\nabla Z \tag{77}$$

from (21), where (76) specifies χ and $\partial n_0/\partial s = 0$ from (39). Reassuringly, the transverse vorticity from (76)–(77),

$$\omega_2 = -\frac{\partial\chi}{\partial s}\frac{dZ}{db} = \frac{Q^*}{q}\frac{dZ}{db}, \tag{78}$$

agrees with the Eq. (56), which we obtained directly from Crocco's theorem.

9. Physical interpretation

We decompose vorticity and other relevant quantities into a baroclinic part (subscript BC) and two barotropic parts according to dependence on environmental streamwise or transverse vorticity (subscripts BTIS or BTIC, respectively). In (27), for example,

$$Q^*_{\rm BTIS} = 0, \quad Q^*_{\rm BTIC} = q_0\frac{dq_0}{dZ}, \quad Q^*_{\rm BC} = -T'\frac{dS}{dZ}. \tag{79}$$

We need the following definitions:

$$E(s,n_0,Z) \equiv \int_{\sigma=0}^{s}\frac{1}{q(\sigma,n_0,Z)}d\sigma \quad \text{and} \tag{80}$$

$$\Lambda(s,n_0,Z) \equiv \int_{0}^{s}\frac{T'(\sigma,n_0,Z)}{q(\sigma,n_0,Z)}d\sigma. \tag{81}$$

Since $d\sigma/q$ is the Lagrangian element of time, E is the time that has elapsed since the parcel at (s, n_0, Z) passed the $s = 0$ transverse, and Λ is the cumulative temperature excess defined by DJ00 for substitution into (21) for baroclinic vorticity (Dutton 1986, p. 389). [Dutton (1986, p. 390) defined Λ as the cumulative temperature but this does not alter $\nabla\Lambda\times\nabla S$ here.] The decomposition of χ in (76) is then

$$\chi_{\rm BTIS} = -q_0\frac{d\beta_0}{dZ}n_0, \quad \chi_{\rm BTIC} = -q_0\frac{dq_0}{dZ}E, \quad \chi_{\rm BC} = \Lambda\frac{dS}{dZ}, \tag{82}$$

where $\chi_{\rm BTIS} + \chi_{\rm BTIC} = M$ in (21). Inserting (82) into (77) gives us a major result: For steady, inviscid, isentropic flow of dry air with zero PV, the vorticity in terms of potentials is

$$\begin{aligned}\boldsymbol{\omega} = &\left(-q_0\frac{d\beta_0}{dZ}\right)\nabla n_0\times\nabla Z - \left(q_0\frac{dq_0}{dZ}\right)\nabla E\times\nabla Z + \left(\frac{dS}{dZ}\right)\nabla\Lambda\times\nabla Z,\\ = &\quad\boldsymbol{\omega}_{\rm BTIS} \qquad\quad +\boldsymbol{\omega}_{\rm BTIC} \qquad\quad +\boldsymbol{\omega}_{\rm BC}\end{aligned} \tag{83}$$

where the quantities in parentheses depend only on Z and can be taken inside the first gradient of each term. This is a three-way partition of vorticity because each individual term can be put in the form of a curl and thus is solenoidal in its own right with its own vector lines. Moreover, each term involves a cross product with ∇Z and so separately conserves (zero) PV. The vorticity is a superposition of a barotropic part $\boldsymbol{\omega}_{\rm BTIS}$ that derives from the environmental streamwise vorticity $-q_0 d\beta_0/dZ$, another barotropic part $\boldsymbol{\omega}_{\rm BTIC}$ arising from the environmental transverse vorticity dq_0/dZ, and a baroclinic part $\boldsymbol{\omega}_{\rm BC}$ that depends on the background stratification dS/dZ and stems from vorticity generated within the storm.

In contrast to the axial vector $\boldsymbol{\omega}$, the barotropic part of the true vector $a\boldsymbol{\omega}$ is frozen into the fluid (Salmon 1998, p. 199). Because $a\boldsymbol{\omega}_{\rm BTIS}$ and $a\boldsymbol{\omega}_{\rm BTIC}$ individually satisfy the homogeneous (barotropic) version of (8), their separate vector lines are frozen into the fluid. Since

$$a\nabla n_0\times\nabla Z = a\frac{\partial n_0}{\partial n}\frac{dZ}{db}\mathbf{t} = \frac{q}{q_0}\mathbf{t}, \tag{84}$$

from (45) and (47),

$$a\boldsymbol{\omega}_{\rm BTIS} = \left(-q_0\frac{d\beta_0}{dZ}\right)\frac{q\mathbf{t}}{q_0} \equiv \lambda_0\mathbf{v} \tag{85}$$

from $a \times$ (83). Thus, $a\boldsymbol{\omega}_{\mathrm{BTIS}}$ is Beltrami (vorticity parallel to wind) with abnormality λ_0 equal to the veering of the environmental wind per unit height. {Note that mass continuity [(2)] and nondivergence of $\boldsymbol{\omega}_{\mathrm{BTIS}}$ requires $\mathbf{v}\cdot\nabla\lambda_0 = 0$ (constancy of abnormality along a streamline), which is satisfied here by $\lambda_0 = \lambda_0(Z)$ and (3).} The vector lines of $\boldsymbol{\omega}_{\mathrm{BTIS}}$ coincide with the flow streamlines so $\boldsymbol{\omega}_{\mathrm{BTIS}}$ has no transverse component, and $|a\boldsymbol{\omega}_{\mathrm{BTIS}}|$ varies as the separation of adjacent parcels on the same streamline. Thus, $\boldsymbol{\omega}_{\mathrm{BTIS}}$ is streamwise vorticity that is imported into the storm from the environment and subsequently stretched by the streamwise-stretching factor $\delta s/a\delta s_0$ or q/aq_0 [see (45)]. The flux of $\boldsymbol{\omega}_{\mathrm{BTIS}}$ along a streamtube is constant. Advection and stretching of $\alpha\boldsymbol{\omega}_{\mathrm{BTIS}}$ sum to zero to preserve the steady state.

The barotropic part of $a\boldsymbol{\omega}$ owing to imported crosswise vorticity is

$$a\boldsymbol{\omega}_{\mathrm{BTIC}} = -\frac{dq_0}{dZ}\nabla E \times (aq_0\nabla Z) \tag{86}$$

from $a \times$ (83), where $aq_0\nabla Z = q\mathbf{b}/R$ from (42). Since $\partial E/\partial s = 1/q$,

$$a\begin{bmatrix}\omega_1\\ \omega_2\end{bmatrix}_{\mathrm{BTIC}} = \begin{bmatrix}-q\dfrac{\delta_\perp E}{\delta_\perp n_0}\\ 1/R\end{bmatrix}\frac{dq_0}{dZ} \tag{87}$$

via (43). A similar derivation for $a\boldsymbol{\omega}_{\mathrm{BC}}$ yields

$$a\begin{bmatrix}\omega_1\\ \omega_2\end{bmatrix}_{\mathrm{BC}} = \begin{bmatrix}q\dfrac{\delta_\perp \Lambda}{\delta_\perp n_0}\\ -T'/R\end{bmatrix}\frac{1}{q_0}\frac{dS}{dZ}. \tag{88}$$

We now examine how the vorticity components vary along streamlines. From (87) and (88) or (57) the transverse vorticity ω_2 is given by

$$a\omega_2 = \frac{1}{q_0 R}\left(q_0\frac{dq_0}{dZ} - T'\frac{dS}{dZ}\right) = \frac{1}{q_0 R}Q^*. \tag{89}$$

It is independent of the environmental streamwise vorticity and consists of two parts (Fig. 7). The barotropic part of $a\omega_2$ equals the environmental transverse vorticity times the local to environmental streamline spacing $1/R$. (Note that $1/R$ is not the same as the inverse wind speed, which is proportional also to the local spacing of the Z surfaces.) The barotropic part is positive (negative) if the storm-relative environmental winds increase (decrease) with height. Since $T' > 0$ (<0) in a downdraft (updraft) and $dS/dZ < 0$ (section 3), the baroclinic transverse vorticity is positive (negative) in a downdraft (updraft). From (57) the overall transverse vorticity is proportional

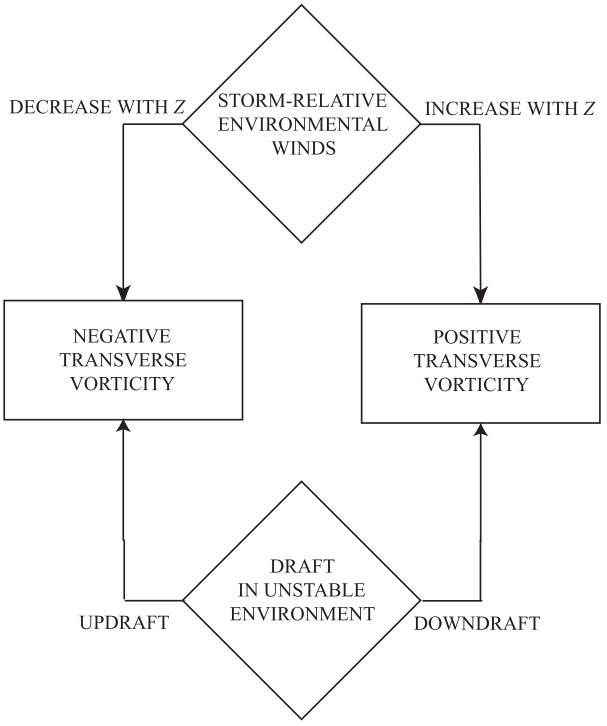

FIG. 7. Diagram illustrating origins of a parcel's transverse vorticity in the idealized flow. Positive (negative) transverse vorticity arises from initial positive (negative) transverse vorticity in the environment and, in an unstable environment, from baroclinic transverse vorticity owing to positive (negative) excess temperature of parcel in the downdraft (updraft). Excess temperature is the temperature of a parcel minus its temperature in the environment.

to and has the same sign as Q^*, which from (79) is the sum of $Q^*_{\mathrm{BTIC}} = q_0 dq_0/dZ$ and $Q^*_{\mathrm{BC}} = -T'\,dS/dZ$.

From (85), (87), (88), (80), and (81) the streamwise vorticity ω_1 is given by

$$a\omega_1 = \lambda_0 q - \frac{dq_0}{dZ}q\frac{\delta_\perp}{\delta_\perp n_0}\int_{\sigma=0}^{s}\frac{1}{q(\sigma, n_0, Z)}d\sigma + \frac{dS}{dZ}\frac{q}{q_0}\frac{\delta_\perp}{\delta_\perp n_0}\int_0^s \frac{T'(\sigma, n_0, Z)}{q(\sigma, n_0, Z)}d\sigma, \tag{90}$$

where the integrals are E and Λ, respectively. Figure 8 summarizes the processes in the idealized flow that result in streamwise vorticity. We have already discussed the first term on the right, the Beltrami term. The second term is the non-Beltrami barotropic streamwise vorticity. It involves the river-bend effect (Shapiro 1972; Scorer 1997; DJ+01). Because there is no vorticity in the binormal direction, the speed of flow with positive curvature increases toward the left [see (53)]. Since the elapsed time E depends on $1/q$, $\delta_\perp E/\delta_\perp n$ is negative. Hence, flow with positive curvature and positive environmental transverse barotropic vorticity (or positive speed shear) produces streamwise vorticity. Vortex lines

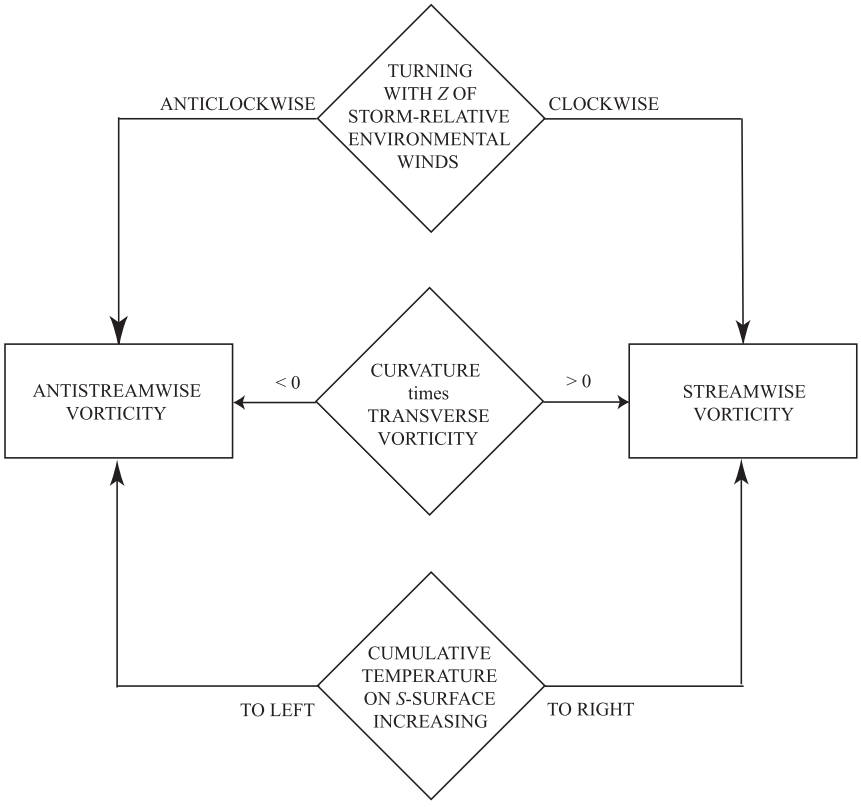

FIG. 8. Illustration of the contributions to a parcel's streamwise (antistreamwise) vorticity in the idealized flow. The contributions are (i) initial streamwise (antistreamwise) vorticity in the environment, (ii) baroclinic vorticity owing to rightward (leftward) gradient of cumulative temperature on the isentropic surface, and (iii) the river-bend effect acting either on positive (negative) transverse vorticity in positively curved flow or on negative (positive) transverse vorticity in negatively curved flow. From a viewpoint above the Z surface, the curvature is positive (negative) for anticlockwise (clockwise) turning flow.

that are initially transverse are turned toward the streamwise direction because in the outer (inner) part of the bend the flow is slower (faster) and because the streamlines are longer (shorter). In steady flow there is no counter process that turns streamwise vorticity into transverse vorticity (Dahl et al. 2014). The third term is the streamwise baroclinic vorticity. It is positive (negative) in unstable stratification if in the isentropic surface the transverse gradient (not the horizontal gradient) of cumulative temperature is to the right (left).

There is a baroclinic river-bend effect as well as a barotropic one. We demonstrate this while discussing the streamwise-vorticity equation [(67)]. The first term is the Beltrami vorticity. It is the homogeneous solution of (66) with the environmental streamwise vorticity as the upstream boundary condition. The curvature forcing term K involves both the barotropic and the baroclinic transverse vorticity. Predominantly through streamwise stretching, the propagator $\Phi(s, \sigma)$ projects forward to the current time the following vorticities: (i) initial streamwise vorticity, (ii) increments of streamwise vorticity that are generated streamwise baroclinically in a negative transverse temperature gradient, (iii) streamwise vorticity increments created barotropically through turning in positively curved flow of positive environmental transverse vorticity, and (iv) streamwise vorticity increments arising from leftward turning of positive transverse baroclinic vorticity generated in a streamwise temperature gradient.

The vertical vorticity in the idealized flow is

$$\zeta = \omega_1 \mathbf{t} \cdot \mathbf{k} + \omega_2 \mathbf{n} \cdot \mathbf{k}. \tag{91}$$

Its dependences on ω_1 and ω_2 are shown in Fig. 9. In steady flow the streamwise vorticity naturally is horizontal at the nadir of a trajectory (where $\mathbf{t} \cdot \mathbf{k} = 0$). Any vertical vorticity at the nadir must be due to transverse vorticity (DJ00). With positive transverse vorticity ($\omega_2 > 0$), the vertical vorticity is positive at streamline nadir points on the left side of a valley in the isentropic surface (where $\mathbf{n} \cdot \mathbf{k} > 0$). Note that these points are still above the surface. Although streamwise vorticity does not contribute to vertical vorticity at the nadir points, it is still very important because it may

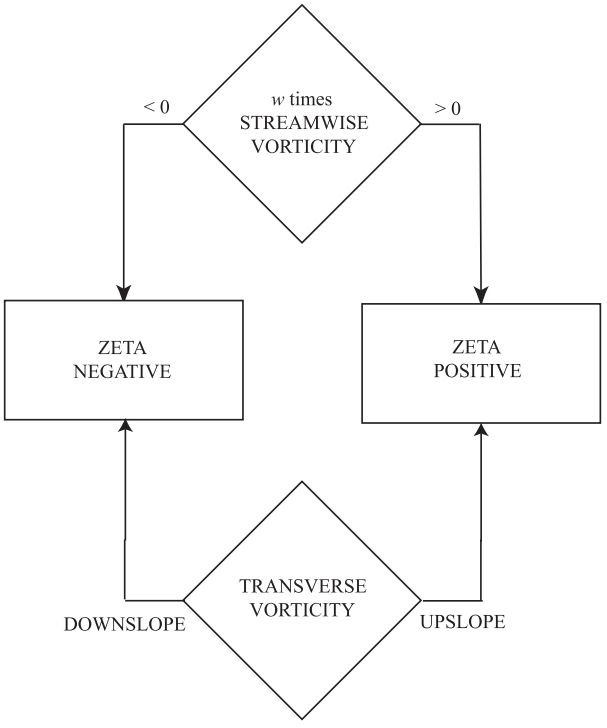

FIG. 9. Origins of a parcel's vertical vorticity ζ in the idealized flow. Positive (negative) ζ in the isentropic surface is due to streamwise (antistreamwise) vorticity pointing upward (downward) along the streamline and to transverse vorticity being directed upslope (downslope). Note that cyclonic vorticity is positive (negative) in the Northern (Southern) Hemisphere.

be associated with rotation at only slightly higher altitudes. This is especially true at the base of a vortex where the streamlines turn abruptly upward and the streamwise direction becomes nearly vertical.

Unfortunately there is no easy way to amend the analysis for conditional instability. Although a case might be made for conservation of an equivalent entropy S_E instead of S and of a corresponding equivalent PV, $\alpha\boldsymbol{\omega}\cdot\nabla S_E$, a difficulty arises because the term for baroclinic generation of vorticity is $\nabla T\times\nabla S$, not $\nabla T\times\nabla S_E$, and this results in nonconservation of (nonzero) PV.

10. Implications for supercells

The direct flux of Beltrami vorticity $\boldsymbol{\omega}_{\mathrm{BTIS}}$ from the environment to the updraft in a steady supercell explains why large environmental near-ground storm-relative streamwise vorticity associates with tornadic storms (Coffer and Parker 2017). The veering of the storm-relative environmental wind per unit height λ_0 next to the ground is typically $\sim 10^{-3}\,\mathrm{m}^{-1}$ in tornado environments. For a relative wind speed of $10\,\mathrm{m\,s}^{-1}$ the associated environmental streamwise vorticity is $10^{-2}\,\mathrm{s}^{-1}$. The copious near-ground streamwise vorticity, modified by streamwise stretching, flows directly along streamlines into the updraft from the warm storm inflow. This process sustains a mesocyclone (threshold vertical vorticity $10^{-2}\,\mathrm{s}^{-1}$) at low altitudes. Because the air is rising, the rotation is above the surface (Davies-Jones 1982).

When the vorticity is partly transverse in the environment, it may still end up predominantly streamwise (or antistreamwise) in a vortex core owing to the curvature term K in (67). From (23) the transverse environmental barotropic vorticity is the storm-relative speed shear. Wicker (1996) ran two simulations that were identical apart from a different wind profile in the lowest 333 m (Fig. 10). The simulation R0 with appreciable low-level hodograph curvature produced a low-level mesocyclone much sooner than R1, which had a comparatively straight hodograph. Figure 11 shows the environmental vorticity components for the two cases. The streamwise vorticity near the ground is positive with minor variations between cases. The most significant differences are in the transverse vorticity. In the lowest 333 m, the transverse vorticity is positive in R0 and negative in R1. [The transverse vorticity dq_0/dz is positive (negative) if the vorticity vector, which is left normal to the hodograph curve, lies to the left (right) of the storm-relative wind vector.] Similarly, Brooks et al. (1993) conducted three simulations, only one of which produced a storm with long-lived low-level rotation. This storm happens to be the one with the most positive near-ground environmental transverse vorticity although admittedly there are other influences. Some tornado-proximity hodographs feature appreciable positive transverse vorticity (e.g., Fig. 5.9b in DJ+01 and Fig. 12 in DJ84). The near-surface positive transverse vorticity is significantly negative in the hodograph in Fig. 14 of DJ84, indicating that the river-bend effect acting on environmental vorticity would delay the development of cyclonic low-level barotropic rotation through tilting of streamwise environmental barotropic vorticity.

Positive (negative) transverse vorticity aids (hinders) formation of near-ground rotation by increasing (deceasing) Q^*. Trajectories descending into a low-level mesocyclone classically pass at low elevations through the hook echo region. The flow here is cyclonically curved with anticyclonic shear vorticity owing to the horizontal pressure gradient force between a mesohigh and the mesocyclone's central mesolow. According to (83) and (87), positive transverse vorticity is turned into streamwise vorticity by the river-bend effect, as happens in the simulations by Adlerman et al. (1999), MR14, and others. This effect augments the streamwise vorticity produced by longitudinal stretching of environmental streamwise vorticity. The combined streamwise vorticity is then tilted upward as parcels stop subsiding and are

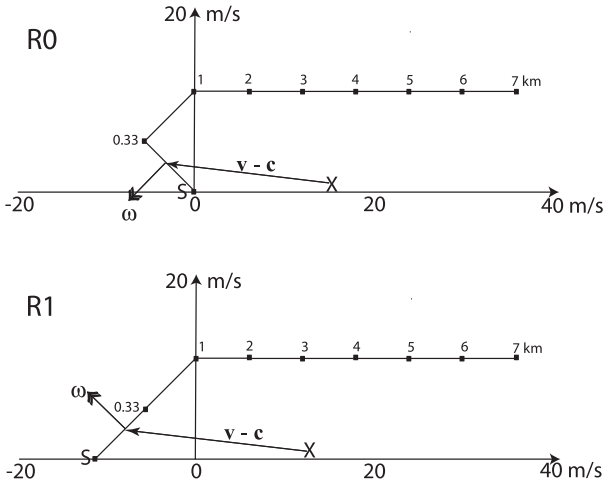

FIG. 10. Hodographs for Wicker's (1996) R0 and R1 simulations. Winds are in m s^{-1} and numbers along the curves at the dots are heights (km). The shear is constant in each height interval. Letters S and X denote the surface wind and the storm motion, respectively. The arrows marked $\boldsymbol{\omega}$ and **v**–**c** are the environmental vorticity and storm-motion vectors, respectively, at a height of 175 m. The 0–1-km storm-relative helicities are 234 $m^2 s^{-2}$ for R0 and 258 $m^2 s^{-2}$ for R1 (adapted from Wicker 1996).

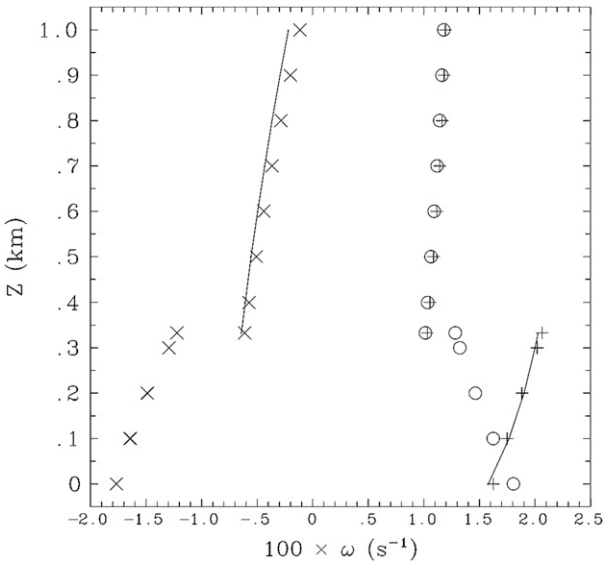

FIG. 11. Crosswise and streamwise environmental vorticity vs height in the lowest kilometer in the R1 and R0 simulations. All the vorticities are discontinuous at 0.33 km AGL. Unconnected plus signs (R1) and circles (R0) mark the quite similar streamwise-vorticity curves for the two simulations. Unconnected crosses (R1) and solid curve without markers (R0) depict the crosswise-vorticity functions, which are very different in the lowest 0.33 km. In this layer the crosswise-vorticity is negative in R1 and positive in R0. Insignificant differences in vorticity above 0.33 km are due solely to small differences in storm motion. Below 0.33 km the crosswise vorticity in R0 and the streamwise vorticity in R1 are almost identical.

drawn upward by the updraft. Conversely, negative transverse vorticity is turned into antistreamwise vorticity, which lessens the overall cyclonic vorticity when tilted. Thus negative transverse vorticity in cyclonically curved flow has the negative effect of delaying vortex formation (DJ+01, Table 5.1). RK85 and Dahl (2015) simulated storms in environments with purely unidirectional shear. The initial storm splits into a severe left supercell (SL) and a severe right-moving supercell (SR). The tip of the storm-motion vectors lies along a perpendicular to the hodograph through a point aloft, which is ~3 km AGL in the above simulations. The transverse environmental vorticity is thus negative in the lowest few kilometers. In flow around the mesocyclone of the SR storm the river-bend effect produces antistreamwise vorticity, which when tipped upward yields anticyclonic vertical vorticity. Stretching of streamwise vorticity does lead to rotation of the correct sign, thus compensating for some of the anticyclonic rotation. However, diagnostic computations show that the overall barotropic rotation is still anticyclonic in unidirectional shear (i.e., in the opposite sense to the actual rotation).

This brings us to the role of baroclinic vorticity. Circulation (RK85, DJB93) and trajectory (MR14; Dahl et al. 2014; Dahl 2015) analyses show that near-ground cyclonic rotation in supercells in all types of shear is due mainly to tilting of baroclinic vorticity in negatively buoyant air in the storm's outflow. DJ+01 (p.182) point out the danger that can be latent in a narrow current of descending cool air. The baroclinic process can overcome eventually the hindrance owing to any negative barotropic river-bend effect because the baroclinic river-bend effect is positive in a mesocyclone. A parcel enters a storm with its environmental vorticity that is subsequently modified by stretching and reorientation owing to barotropic vorticity being frozen in the fluid and accumulates baroclinic vorticity over time through the actions of buoyancy torques. Each increment of vorticity that is generated during a small time interval in the past is propagated barotropically forward in time, and the net baroclinic vorticity of the parcel at a current time is the vector sum of all these propagated vorticity increments. In an isentropic surface a parcel has a positive temperature excess T' if it is at a lower altitude than its environmental height. Thus, the transverse baroclinic vorticity is positive in a steady negatively buoyant downdraft and is turned into streamwise vorticity in cyclonically curved flow as observed along important trajectories in simulations of Adlerman et al. (1999) and MR14. Moreover, the parcel entering a near-ground cyclone typically passes along a subsidence gradient in the hook echo region with the greatest temperature excesses in the surface to its right. Additional streamwise vorticity is thereby produced. Subsequent upward tilting of the total streamwise vorticity in the corner region of the vortex produces cyclonic rotation.

The presence of the Beltrami partial vorticity in steady flow removes one objection to the use of Beltrami flows in approximate modeling of supercell updrafts (Weisman and Rotunno 2000), namely that a pure Beltrami flow is impossible in the presence of buoyancy forces (Lilly 1986). Owing to the Beltrami partial vorticity, Beltrami-flow characteristics still are conspicuous in observed and simulated supercells in directional shear (Lilly 1986). The existence of a Beltrami part to the asymptotic barotropic vorticity field vindicates the use of Beltrami flows for analytical description of rotating updrafts in environments with arc-shaped hodograph curves that turn clockwise significantly with height and storm motion fairly near the center of curvature. Figures 9–11, 13, and 15 of DJ84 are examples of tornadic-storm environments with large storm-relative streamwise vorticity and little transverse vorticity near the surface.

A more serious objection to Beltrami flows is that, when the inviscid flow is unsteady, the Beltrami part is no longer a solution of the homogeneous vorticity equation and the decomposition of barotropic vorticity into streamwise and transverse partial vorticities fails. But a supercell is long lived and quasi steady so the steady assumption is a reasonable starting point for describing a supercell. Moreover, the Beltrami vorticity is an equilibrium solution of the barotropic vorticity equation. If this equilibrium is stable, then there exist unsteady solutions for barotropic vorticity that stay close to the Beltrami vorticity.

Linear theory provides a simple way to incorporate unsteadiness by assuming a form-preserving disturbance (FPD) with constant growth rate and motion vector (DJ84; Kanak and Lilly 1996). In the case with purely streamwise vorticity, growth decorrelates vorticity and velocity. This is because a small (material) segment AB of a barotropic vortex line that is along a streamline (i.e., streamwise) in the environment moves off this streamline inside an evolving storm because parcels A and B move along their trajectories, which are not streamlines in unsteady flow. For |Richardson number| ≤ 1, vertical vorticity and vertical wind remains highly correlated nevertheless.

An FPD has an unambiguous storm motion, which allows for precise definition of storm-relative quantities. There is a type of nonlinear FPD that, like an evolving supercell, has large initial growth and variable motion diminishing toward an asymptotic steady state with constant amplitude and motion vector (Kanehisa 2002). Time-varying growth rate and motion prevents the cell from becoming deformed. Davies-Jones (2002) found that wider updrafts propagate further off a curved hodograph (to the concave side) and are less susceptible to deformation than narrower ones. Unfortunately a Beltrami flow, being inherently steady (or viscously decaying), is not of this type.

However, supercells are not exactly FPDs. They do not preserve their shape either during their formative stages or during tornadogenesis. Consider, for example, a storm in an environment with a semicircular hodograph curve. As the supercell intensifies, several changes occur to sustain it. The storm motion deviates toward the center of curvature, which makes the storm-relative environmental vorticity more streamwise. The upward dynamic pressure gradient force associated with upward increasing rotation in the mesocyclone [i.e., vortex suction (Lilly 1986)] lifts low-level air (MR14), thereby strengthening the updraft and associated low-level convergence. The streamtubes are stretched further, thereby increasing the low-level rotation and deepening the mesolow. As the storm strengthens, the trajectories in the mesocyclone become more curved, the baroclinic zone intensifies, and the river-bend effect, which still functions in unsteady flow, turns crosswise vorticity into streamwise vorticity, which further enhances low-level rotation when tilted upward.

The form-preserving assumption prevents a maximum in rotation from lowering to the ground and also the formation of a new maximum. The dynamic-pipe effect (Smith and Leslie 1979; Trapp and Davies-Jones 1997) is one mechanism by which a rotation maximum can descend. A new maximum can form also as a result of descending rotating flow interacting with the ground. The basic process works regardless of the presence or absence of friction forces. In a balanced flow with purely streamwise vorticity, the vortex lines and trajectories are aligned. Rotation closer to the ground can be produced through separation of the vortex lines and trajectories. In the DJB93 mechanism (sections 1 and 4), baroclinic generation of horizontal vorticity inclines the vortex lines upward relative to the trajectories. Conversely, in the axisymmetric simulation of DJ08, precipitation drag inclines the trajectories downward relative to the vortex lines with the same net effect. In the DJ08 model, angular momentum is approximately conserved and vanishes at the ground owing to the initial condition. It serves as a vortex-line function for the radial-vertical vorticity. Precipitation drag augments an annular downdraft surrounding an axial updraft. The downdraft boost lowers and concentrates angular-momentum surfaces, thus greatly amplifying inward vorticity already present. Some of the outflow air from the downdraft is directed inward toward the axis. The negatively buoyant air, if not too stable (Markowski et al. 2003b), is subsequently drawn upward in the axial updraft. Owing to upward tipping of the inward vorticity, a tornado forms within the mesocyclone, thus completing a vortex column from the ground to a great height (DJ+01). Friction aids the process by decelerating the tangential flow near the ground, generating further inward vorticity. It also causes cyclostrophic

imbalance, which drives air in the vortex boundary layer inward. Even though this air has relatively low angular momentum, it spins up into a tornado owing to its close approach to the axis.

In terms of this paper's theory, the process is not so clear cut because the flow is less constrained and the conserved variables are entropy and zero PV. The flow is steady so we can only consider how a tornado is maintained, not how it forms. The ground is an immovable horizontal isentropic surface. As in DJ08 there is no rotation at the ground. However, rotation can still be present just above the ground through stretching of streamwise vorticity along trajectories that turn cyclonically and descend before turning abruptly upward into a tornado (like in DJ08). How does the tornado maintain its large vorticity? First the river-bend effect turns positive transverse vorticity toward the streamwise direction. Second, since the ground is a fixed isentropic surface, downward depression of the isentropic surfaces aloft greatly amplifies the packing (inverse spacing) dZ/db of the surfaces. By mass conservation

$$\frac{dZ}{db} = \frac{\alpha_0}{\alpha}\frac{q}{q_0}\frac{1}{R} \tag{92}$$

from (42), where $1/R$ is the ratio of local to environmental streamline spacing. Large dZ/db relates to large $\alpha_0 q/\alpha q_0$ and/or to comparatively large streamline spacing. Since B is constant on an isentropic surface,

$$\frac{q^2 - q_0^2}{2} + c_p(T - T_0) + g(z - Z) = 0. \tag{93}$$

A parcel that enters a tornado gains specific kinetic energy at the expense of static energy $c_pT + gz$ (Davies-Jones 2015a). It is in a favorable pressure gradient as low pressure is ahead. Thus, the large increase in dZ/db as it nears the ground associates with large q/aq_0 rather than large $1/R$, which would tend to increase transverse vorticity [see (57)]. The tornado obtains its abundant streamwise vorticity through streamwise stretching [see (67)] caused by isentrope packing.

What happens if diabatic heating/cooling is included? The barotropic PV, $Q_{\mathrm{BT}} \equiv \alpha\boldsymbol{\omega}_{\mathrm{BT}}\cdot\nabla Z$, is still conserved and zero if the environment is horizontally uniform. So the barotropic vorticity still does not have a binormal component on Z surfaces and in particular a vertical component on flat ground. With diabatic heating/cooling S is no longer a function of just Z and the isentropic surfaces can intersect the ground. Moreover, $\alpha\boldsymbol{\omega}_{\mathrm{BC}}\cdot\nabla S$ is no longer conserved and zero so the baroclinic vortex lines are not constrained to lie in the isentropic surfaces. Rotation on the ground is now possible because the baroclinic vortex lines can terminate on the ground.

11. Conclusions

In idealized, steady, inviscid, isentropic inflows of dry air from a horizontally uniform environment, the vorticity field $\boldsymbol{\omega}$ consists of barotropic vorticity arising from imported streamwise vorticity $\boldsymbol{\omega}_{\mathrm{BTIS}}$, barotropic vorticity stemming from imported crosswise vorticity $\boldsymbol{\omega}_{\mathrm{BTIC}}$, and baroclinic vorticity $\boldsymbol{\omega}_{\mathrm{BC}}$. In steady flow $\boldsymbol{\omega}_{\mathrm{BTIS}}$ is Beltrami (always parallel to the 3D wind). The streamlines and vortex lines lie in the stationary isentropic surfaces so there are only two independent components: streamwise and transverse. The transverse component of a parcel's vorticity arises from imported environmental transverse vorticity and from baroclinic vorticity generated incrementally while it is in streamwise temperature gradients. The propagator for transverse vorticity is the local streamline spacing divided by the environmental spacing.

The streamwise component of a parcel's vorticity derives from imported environmental streamwise vorticity, from baroclinic vorticity generated while it is in negative transverse temperature gradients, and from environmental and baroclinic positive transverse vorticity that is turned into the streamwise direction in cyclonically curved flow. Stretching along the streamlines propagates each increment of the parcel's streamwise vorticity forward to the current time. Enlargement of streamwise vorticity in subsiding air near the ground is probably an important factor in tornadogenesis. The Beltrami part of the barotropic vorticity is purely streamwise vorticity that is imported from the environment and stretched. It explains why abundant environmental storm-relative streamwise vorticity close to the ground favors tornadic supercells. This vorticity flows directly into the base of the storm updraft unmodified apart from streamwise stretching, thus maintaining mesocyclonic rotation at low altitudes.

In steady cyclonically curved subsiding low-altitude flow around the mesocyclone core, turning of positive, mainly baroclinic (or frictional), transverse vorticity augments streamwise vorticity by a river-bend effect. For storms in environments where the transverse environmental vorticity is positive (negative) at low elevations, this effect is enhanced (reduced) because positive (negative) environmental transverse vorticity is turned into streamwise (antistreamwise) vorticity in cyclonically curved flow.

Acknowledgments. Special thanks to Dr. Qin Xu for carefully checking the derivations. Dr. Paul Markowski provided valuable insights into the interpretation. Longago conversations with Drs. Harold Brooks and Louis Wicker were also perceptive. The paper benefited from the comments of Dr. Richard Rotunno and two other formal reviewers. The author performed this work as a NOAA

Scientist Emeritus. The National Severe Storms Laboratory paid the publication costs.

APPENDIX A

Constants of Motion in Steady Inviscid Flow

Let $Q^\dagger = a\boldsymbol{\omega}\cdot\nabla\Theta$, where Θ is any conserved variable (such that $\mathbf{v}\cdot\nabla\Theta = 0$) and $Q^\dagger$ is a generalized PV. By (2), (7), (14), and vector identities,

$$\begin{aligned}(\mathbf{v}/a)\cdot\nabla Q^\dagger &= \nabla\cdot(Q^\dagger\mathbf{v}/a) = \nabla\cdot[(\nabla\Theta\cdot\boldsymbol{\omega})\mathbf{v}]\\ &= -\nabla\cdot[\nabla\Theta\times(\boldsymbol{\omega}\times\mathbf{v})] = \nabla\Theta\cdot\nabla\times(\boldsymbol{\omega}\times\mathbf{v})\\ &= \nabla\Theta\cdot(\nabla T\times\nabla S).\end{aligned} \tag{A1}$$

When $\Theta = Z(S)$, the right side vanishes, thus proving the invariance of the customary PV Q along streamlines. Choosing $\Theta = \psi$ instead yields

$$\mathbf{v}\cdot\nabla Q^* \equiv \mathbf{v}\cdot\nabla(a\boldsymbol{\omega}\cdot\nabla\psi) = a\nabla\psi\cdot(\nabla T\times\nabla S). \tag{A2}$$

The barotropic part of Q^*, $a\boldsymbol{\omega}_{\rm BT}\cdot\nabla\psi$, satisfies $\mathbf{v}\cdot\nabla Q^*_{\rm BT} = 0$ and so is invariant along streamlines.

APPENDIX B

Commutation Relation

We start with the vector identity $\nabla\times\nabla\phi = 0$, where ϕ is any twice continuously differentiable scalar. In (s, n_0, Z) coordinates, this is

$$\left(\mathbf{t}\frac{\partial}{\partial s} + \mathbf{n}\frac{\delta_\perp}{\delta_\perp n} + \mathbf{b}\frac{\partial}{\partial b}\right)\times\left(\frac{\partial\phi}{\partial s}\mathbf{t} + \frac{\delta_\perp\phi}{\delta_\perp n}\mathbf{n} + \frac{\partial\phi}{\partial b}\mathbf{b}\right) = 0 \tag{B1}$$

by (50). Taking the dot product with $\mathbf{b}$ gives us

$$\begin{aligned}0 = {}& \frac{\partial}{\partial s}\left(\frac{\delta_\perp\phi}{\delta_\perp n}\right) - \frac{\delta_\perp}{\delta_\perp n}\left(\frac{\partial\phi}{\partial s}\right) + \frac{\partial\phi}{\partial s}\mathbf{b}\cdot\left(\mathbf{t}\times\frac{\partial\mathbf{t}}{\partial s} + \mathbf{n}\times\frac{\delta_\perp\mathbf{t}}{\delta_\perp n}\right)\\ &+ \frac{\delta_\perp\phi}{\delta_\perp n}\mathbf{b}\cdot\left(\mathbf{t}\times\frac{\partial\mathbf{n}}{\partial s} + \mathbf{n}\times\frac{\delta_\perp\mathbf{n}}{\delta_\perp n}\right)\\ &+ \frac{\partial\phi}{\partial b}\mathbf{b}\cdot\left(\mathbf{t}\times\frac{\partial\mathbf{b}}{\partial s} + \mathbf{n}\times\frac{\delta_\perp\mathbf{b}}{\delta_\perp n}\right).\end{aligned} \tag{B2}$$

With use of (48) and (49), we get

$$\begin{aligned}&\frac{\delta_\perp}{\delta_\perp n}\left(\frac{\partial\phi}{\partial s}\right) - \frac{\partial}{\partial s}\left(\frac{\delta_\perp\phi}{\delta_\perp n}\right) = \frac{\partial\phi}{\partial s}\left(\frac{\partial\mathbf{t}}{\partial s}\cdot\mathbf{b}\times\mathbf{t} - \frac{\delta_\perp\mathbf{t}}{\delta_\perp n}\cdot\mathbf{n}\times\mathbf{b}\right) + \frac{\delta_\perp\phi}{\delta_\perp n}\left(\frac{\partial\mathbf{n}}{\partial s}\cdot\mathbf{b}\times\mathbf{t} - \frac{\delta_\perp\mathbf{n}}{\delta_\perp n}\cdot\mathbf{n}\times\mathbf{b}\right)\\ &\quad + \frac{\partial\phi}{\partial b}\left(\frac{\partial\mathbf{b}}{\partial s}\cdot\mathbf{b}\times\mathbf{t} - \frac{\delta_\perp\mathbf{b}}{\delta_\perp n}\cdot\mathbf{n}\times\mathbf{b}\right) = \frac{\partial\phi}{\partial s}\frac{\partial\mathbf{t}}{\partial s}\cdot\mathbf{n} - \frac{\delta_\perp\phi}{\delta_\perp n}\frac{\partial_\perp\mathbf{n}}{\partial n}\cdot\mathbf{t} + \frac{\partial\phi}{\partial b}\left(\frac{\partial\mathbf{b}}{\partial s}\cdot\mathbf{n} - \frac{\delta_\perp\mathbf{b}}{\delta_\perp n}\cdot\mathbf{t}\right)\\ &\quad = \kappa\frac{\partial\phi}{\partial s} + \frac{\delta_\perp\phi}{\delta_\perp n}\frac{\delta_\perp\mathbf{t}}{\delta_\perp n}\cdot\mathbf{n} + \frac{\partial\phi}{\partial b}\left(\frac{\delta_\perp\mathbf{t}}{\delta_\perp n}\cdot\mathbf{b} - \frac{\partial\mathbf{n}}{\partial s}\cdot\mathbf{b}\right).\end{aligned} \tag{B3}$$

From (48) and (64), we obtain

$$\frac{\delta_\perp}{\delta_\perp n}\left(\frac{\partial\phi}{\partial s}\right) - \frac{\partial}{\partial s}\left(\frac{\delta_\perp\phi}{\delta_\perp n}\right) = \kappa\frac{\partial\phi}{\partial s} - \frac{1}{R}\frac{\partial R}{\partial s}\frac{\delta_\perp\phi}{\delta_\perp n} \tag{B4}$$

or

$$\frac{\partial}{\partial s}\left(\frac{1}{R}\frac{\delta_\perp\phi}{\delta_\perp n}\right) = \frac{1}{R}\left[\frac{\delta_\perp}{\delta_\perp n}\left(\frac{\partial\phi}{\partial s}\right) - \kappa\frac{\partial\phi}{\partial s}\right], \tag{B5}$$

which in (s, n_0, Z) coordinates simplifies via (43) and (53) to the commutation relation

$$\frac{\partial}{\partial s}\left(\frac{\delta_\perp\phi}{\delta_\perp n_0}\right) = \frac{\delta_\perp}{\delta_\perp n_0}\left(\frac{\partial\phi}{\partial s}\right) - \frac{1}{q}\frac{\delta_\perp q}{\delta_\perp n_0}\frac{\partial\phi}{\partial s}. \tag{B6}$$

REFERENCES

Adlerman, E. J., K. K. Droegemeier, and R. Davies-Jones, 1999: A numerical simulation of cyclic mesocyclogenesis. *J. Atmos. Sci.*, **56**, 2045–2069, doi:10.1175/1520-0469(1999)056<2045:ANSOCM>2.0.CO;2.

Batchelor, G. K., 1967: *An Introduction to Fluid Dynamics.* Cambridge University Press, 615 pp.

Borisenko, A. I., and I. E. Tarapov, 1979: *Vector and Tensor Analysis with Applications.* Dover, 257 pp.

Brooks, H.E., C. A. Doswell III, and R. Davies-Jones, 1993: Environmental helicity and evolution of low-level mesocyclones. *The Tornado: Its Structure, Dynamics, Prediction, and Hazards*, *Geophys. Monogr.*, Vol. 79, Amer. Geophys. Union, 97–104.

Coffer, B. E., and M. D. Parker, 2017: Simulated supercells in nontornadic and tornadic VORTEX2 environments. *Mon. Wea. Rev.*, **145**, 149–180, doi:10.1175/MWR-D-16-0226.1.

Dahl, J. M. L., 2015: Near-ground rotation in simulated supercells: On the robustness of the baroclinic mechanism. *Mon. Wea. Rev.*, **143**, 4929–4942, doi:10.1175/MWR-D-15-0115.1.

——, M. D. Parker, and L. J. Wicker, 2014: Imported and storm-generated near-ground vertical vorticity in a simulated supercell. *J. Atmos. Sci. Rev.*, **71**, 3027–3051, doi:10.1175/JAS-D-13-0123.1.

Davies-Jones, R. P., 1982: Observational and theoretical aspects of tornadogenesis. *Intense Atmospheric Vortices*, L. Bengtsson and J. Lighthill, Eds., Springer-Verlag, 175–189.

——, 1984: Streamwise vorticity: The origin of updraft rotation in supercell storms. *J. Atmos. Sci.*, **41**, 2991–3006, doi:10.1175/1520-0469(1984)041<2991:SVTOOU>2.0.CO;2.

——, 2000: A Lagrangian model for baroclinic genesis of mesoscale vortices. Part I: Theory. *J. Atmos. Sci.*, **57**, 715–736, doi:10.1175/1520-0469(2000)057<0715:ALMFBG>2.0.CO;2.

——, 2002: Linear and nonlinear propagation of supercell storms. *J. Atmos. Sci.*, **59**, 3178–3205, doi:10.1175/1520-0469(2003)059<3178:LANPOS>2.0.CO;2.

——, 2004: Growth of circulation around supercell updrafts. *J. Atmos. Sci.*, **61**, 2863–2876, doi:10.1175/JAS-3341.1.

——, 2006: Integrals of the vorticity equation. Part I: General three- and two-dimensional flows. *J. Atmos. Sci.*, **63**, 598–610, doi:10.1175/JAS3646.1.

——, 2008: Can a descending rain curtain in a supercell instigate tornadogenesis barotropically? *J. Atmos. Sci.*, **65**, 2469–2497, doi:10.1175/2007JAS2516.1.

——, 2015a: A review of supercell and tornado dynamics. *Atmos. Res.*, **158–159**, 274–291, doi:10.1016/j.atmosres.2014.04.007.

——, 2015b: Formulas for parcel velocity and vorticity in a rotating Cartesian coordinate system. *J. Atmos. Sci.*, **72**, 3908–3922, doi:10.1175/JAS-D-15-0015.1.

——, and H.E. Brooks, 1993: Mesocyclogenesis from a theoretical perspective. *The Tornado: Its Structure, Dynamics, Prediction, and Hazards, Geophys. Monogr.*, Vol. 79, Amer. Geophys. Union, 105–114.

——, and Y. P. Richardson, 2002: An exact anelastic Beltrami-flow solution for use on model validation. Preprints, *19th Conf. Weather Analysis and Forecasting/15th Conf. Numerical Weather Prediction*, San Antonio, TX, Amer. Meteor. Soc., P1.3. [Available online at https://ams.confex.com/ams/SLS_WAF_NWP/techprogram/paper_47661.htm.]

——, and P. Markowski, 2013: Lifting of ambient air by density currents in sheared environments. *J. Atmos. Sci.*, **70**, 1204–1215, doi:10.1175/JAS-D-12-0149.1.

——, R. J. Trapp, and H. B. Bluestein, 2001: Tornadoes and tornadic storms. *Severe Convective Storms*, *Meteor. Monogr.*, No. 50, Amer. Meteor. Soc., 167–221.

Dutton, J. A., 1986: *The Ceaseless Wind.* Dover, 617 pp.

Epifanio, C. C., and D. R. Durran, 2002: Lee-vortex formation in free-slip stratified flow over ridges. Part II: Mechanism of vorticity and PV production in nonlinear viscous wakes. *J. Atmos. Sci.*, **59**, 1166–1181, doi:10.1175/1520-0469(2002)059<1166:LVFIFS>2.0.CO;2.

Farlow, S. J., 1993: *Partial Differential Equations for Scientists and Engineers.* Dover, 414 pp.

Kanak, K. M., and D. K. Lilly, 1996: The linear stability and structure of convection in a circular mean shear. *J. Atmos. Sci.*, **53**, 2578–2593, doi:10.1175/1520-0469(1996)053<2578:TLSASO>2.0.CO;2.

Kanehisa, H., 1996: A relationship between the Bernoulli function and potential vorticity. *J. Meteor. Soc. Japan*, **74**, 383–386, doi:10.2151/jmsj1965.74.3_383.

——, 2002: A nonlinear extension of the helicity formula for convective storms. *J. Meteor. Soc. Japan*, **80**, 1301–1306, doi:10.2151/jmsj.80.1301.

Kis, A. K., J. M. Straka, K. M. Kanak, and R. P. Davies-Jones, 2008: On the role of descending rain curtains in tornadogenesis. *24th Conf. on Severe Local Storms*, Savannah, GA, Amer. Meteor. Soc., 14.1. [Available online at https://ams.confex.com/ams/24SLS/techprogram/paper_142115.htm.]

Lilly, D. K., 1982: The development and maintenance of rotation in convective storms. *Intense Atmospheric Vortices*, L. Bengtsson and J. Lighthill, Eds., Springer-Verlag, 149–160.

——, 1986: The structure, energetics and propagation of rotating convective storms. Part II: Helicity and storm stabilization. *J. Atmos. Sci.*, **43**, 126–140, doi:10.1175/1520-0469(1986)043<0126:TSEAPO>2.0.CO;2.

Markowski, P. M., and Y. P. Richardson, 2014: The influence of environmental low-level shear and cold pools on tornadogenesis: Insights from idealized simulations. *J. Atmos. Sci.*, **71**, 243–275, doi:10.1175/JAS-D-13-0159.1.

——, J. M. Straka, and E. N. Rasmussen, 2002: Direct surface thermodynamic observations within the rear-flank downdrafts of nontornadic and tornadic supercells. *Mon. Wea. Rev.*, **130**, 1692–1721, doi:10.1175/1520-0493(2002)130<1692:DSTOWT>2.0.CO;2.

——, C. Hannon, J. Frame, A. Pietrycha, R. Edwards, and R. L. Thompson, 2003a: Characteristics of vertical wind profiles near supercells obtained from the Rapid Update Cycle. *Wea. Forecasting*, **18**, 1262–1272, doi:10.1175/1520-0434(2003)018<1262:COVWPN>2.0.CO;2.

——, J. M. Straka, and E. N. Rasmussen, 2003b: Tornadogenesis resulting from the transport of circulation by a downdraft: Idealized numerical simulations. *J. Atmos. Sci.*, **60**, 795–823, doi:10.1175/1520-0469(2003)060<0795:TRFTTO>2.0.CO;2.

——, ——, ——, R. P. Davies-Jones, Y. Richardson, and J. Trapp, 2008: Vortex lines within low-level mesocyclones obtained from pseudo-dual-Doppler radar observations. *Mon. Wea. Rev.*, **136**, 3513–3535, doi:10.1175/2008MWR2315.1.

——, and Coauthors, 2012: The pretornadic phase of the Goshen County, Wyoming, supercell of 5 June 2009 intercepted by VORTEX2. Part II: Intensification of low-level rotation. *Mon. Wea. Rev.*, **140**, 2916–2938, doi:10.1175/MWR-D-11-00337.1.

Mathews, J., and R. L. Walker, 1965: *Mathematical Methods of Physics.* W. A. Benjamin, 475 pp.

Rotunno, R., and J. B. Klemp, 1985: On the rotation and propagation of simulated supercell thunderstorms. *J. Atmos. Sci.*, **42**, 271–292, doi:10.1175/1520-0469(1985)042<0271:OTRAPO>2.0.CO;2.

Salmon, R., 1998: *Geophysical Fluid Dynamics*. Oxford University Press, 378 pp.

Schenkman, A., M. Xue, and M. Hu, 2014: Tornadogenesis in a high-resolution simulation of the 8 May 2003 Oklahoma City supercell. *J. Atmos. Sci.*, **71**, 130–154, doi:10.1175/JAS-D-13-073.1.

Scorer, R. S., 1997: *Dynamics of Meteorology and Climate.* Praxis, 686 pp.

Shapiro, A. H., 1972: Vorticity. *Illustrated Experiments in Fluid Mechanics: The NCFMF Book of Film Notes*, MIT Press, 63–74. [Available online at http://web.mit.edu/hml/ncfmf/09VOR.pdf.]

Smith, R. K., and L. M. Leslie, 1979: A numerical study of tornadogenesis in a rotating thunderstorm. *Quart. J. Roy. Meteor. Soc.*, **105**, 107–127, doi:10.1002/qj.49710544308.

Trapp, R. J., and R. Davies-Jones, 1997: Tornadogenesis with and without a dynamic pipe effect. *J. Atmos. Sci.*, **54**, 113–133, doi:10.1175/1520-0469(1997)054<0113:TWAWAD>2.0.CO;2.

Weisman, M. L., and R. Rotunno, 2000: The use of vertical wind shear versus helicity in interpreting supercell dynamics. *J. Atmos. Sci.*, **57**, 1452–1472, doi:10.1175/1520-0469(2000)057<1452:TUOVWS>2.0.CO;2.

Wicker, L. J., 1996: The role of near-surface wind shear on low level mesocyclone generation and tornadoes. Preprints, *18th Conf. Severe Local Storms*, San Francisco, CA, Amer. Meteor. Soc., 115–119.